Managing pressures in Nedmag caverns to prevent brine leakage during the mining and bleed-off phase and an evaluation of post abandonment cavern behaviour

Consultant: Well Engineering Partners B.V., Hoogeveen

Author:

Version: Final version

Date: 23 November 2018

Summary

Nedmag operates a cavern field applying solution mining of magnesium chloride salts. In contrast to most solution mining operations worldwide, targeting sodium chloride (halite / rocksalt). Due to the thin bedding of magnesium salts (mainly bischofite) and high solubility, the caverns become disk shaped, rather than the typical spherical or cylindrical shapes of rocksalt caverns, stretching many hundreds in metres in diameter, although it is expected that the caverns have a cave-complex or labyrinth type of structure rather than a disk shape, given the non-homogeneous bedding of bischofite within thin carnallite and halite interlayers.

The magnesium salts, mainly bischofite, are also highly mobile, in that they creep fast under small shear loads. This leads to significant cavern convergence if the brine pressures are some MPa's below the lithostatic pressure. Most cavern brine can be collected at surface by allowing low cavern pressures, ultimately resulting in significant surface subsidence.

From a leakage incident in April 2018, it is realized that hydrofractures can occur at brine pressures (well) below lithostatic. This report focusses on the quantification of this effect, to explain the brine leakage and to make sure the pressure regime of future solution mining is tuned to this effect.

This study shows that a relatively thin halite caprock of a cavern (thinner than the lateral dimension of the cavern) can incur a significant drop in stresses due to creep relaxation, if the cavern pressure is well below lithostatic for a significant time (years). The lithostatic stress is the stress that is in balance with the weight of the overburden, which is usually close to 0.021-0.022 MPa per metre depth, and the original salt stress, confirmed by Leak Off Tests (LOT) in salt.

Due to prolonged (decades) low pressure mining in the caverns, the vertical stresses in the salt roof get adjusted to a value somewhere halfway the fluid pressure and vertical stress in the overburden. The latter drops towards the fluid pressure level due to arching effects. The lateral salt stresses adjust to the vertical stress level by salt creep, provided the low pressure period is long enough (years). The lateral stress increase around the cavern due to arching is only temporarily taken up by the salt roof, since it can escape the stress field by creep, transferring the stress to the elastic overburden (Buntsandstone). When the cavern fluid pressure is subsequently increased again (by an increased level of water injection or decreased level of production) the salt stresses do not fully return and a hydrofracture can occur, at cavern fluid pressures that are 5 to 8 MPa below the original salt stress level (the lithostatic level).

In this report a Finite Element simulation (in axi-symmetric 2D and full 3D) is run, to quantify the stress changes in the salt, in order to define the operational pressures in the cavern. Adopting to this pressure regime (with a fluid pressure dropping in time and limited pressure increases due to operations) should preclude future cavern leakages by the formation of hydrofractures. The low pressure also makes sure that the total volume of brine that is left in the salt at the moment of well and cavern abandonment is as small as practically possible. In a post-abandonment situation, some leakage will occur by rising cavern pressures, but the quantities (per time unit) will be much smaller than during the incident of April 2018. As a result of this it is very unlikely that brine or oil can find their way to the sweet water layers (0-250 m) that are (or can be) used for agricultural water extraction. Subsidence rates due to post-abandonment leakage will be negligible if all brine is allowed to be produced until the moment of practical limits (some 2 m^3/h at brine hydrostatic pressures) to maintain a well.

1 Background

Nedmag operates a solution mining plant at the west-side of the city of Veendam (within the municipality of Veendam in the villages Borgercompagnie and Tripscompagnie. They extract, magnesium-chloride brine. The magnesium bearing salts (bischofite, $MgCl_2.6H_2O$, carnallite ($MgKCl_3.6H_2O$) and kieserite ($MgSO_4.H_2O$)) are being dissolved by water injection. A brine with a high level of $MgCl_2$ and low level of other salts is being produced, where most of the others salts within the formations are left behind in the cavern, either remaining at the cavern wall or precipitating (falling down or recrystallizing) at the caverns base (sump) as halite (NaCl), anhydrite ($CaSO_4$), carnallite, sylvite (KCl) or kieserite.

Thirteen wells have been drilled. Four from Well Head Centre 1 at Borgercompagnie (WHC-1: VE-1 to VE-4), 9 from Well Head Centre 2 at Tripscompagnie (Wells TR-1 to TR-9). Four new wells are planned to be drilled from WHC-1 in 2019 and later (VE-5 to VE-8).
Due to selective mining, the cavern shape is less well defined compared to solution mining in relatively pure halite (NaCl) formations. The cavern will have a shape of a cave complex instead. Nine caverns have interconnected through the years by (assumed) selective bischofite dissolution (TR-1 until TR-8 and VE-4, as depicted on Figure 1.

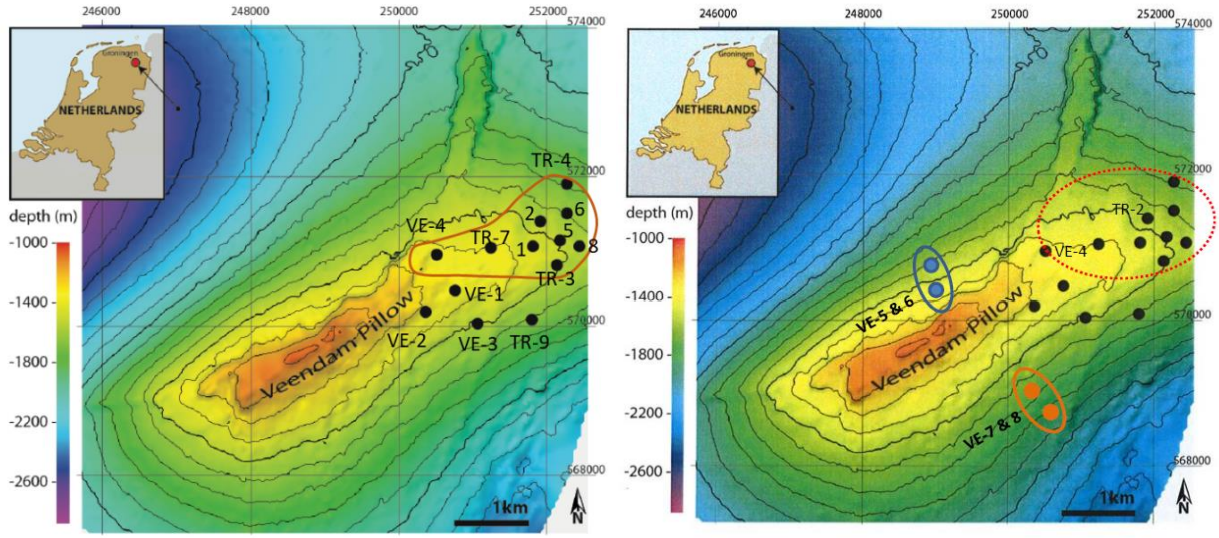

Figure 1: Left: Position of caverns (casing shoes) projected on a depth map of top Zechstein (grid size 2x2 km). The Area inside the solid red line is an indication of the area where the cavern cluster is located. Right: the same casing shoe locations, including the projected wells VE5-6-7-8, that are 1000-2000 meters away from the nearest cavern cluster brine volume.

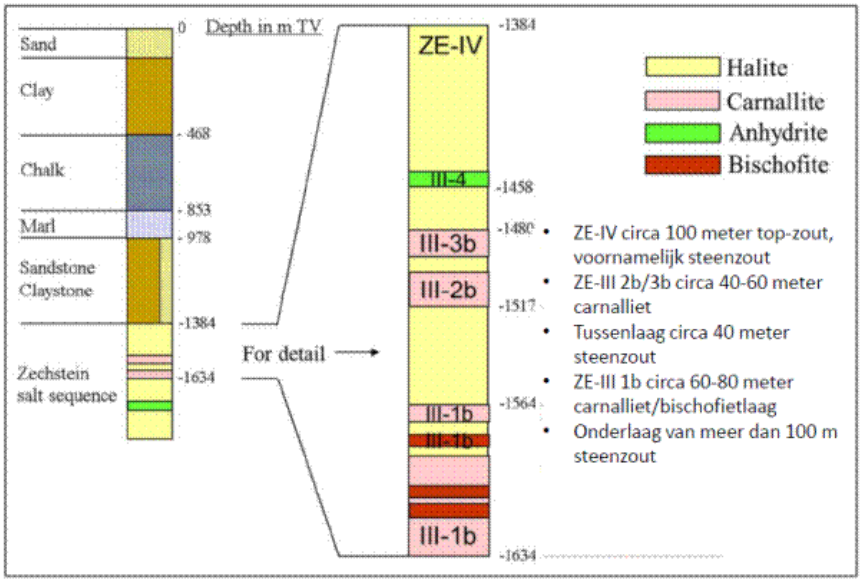

Figure 2: Approximate stratification of the salt and overburden for the Nedmag wells. Depths differ by up to 200 metres, depending on the well's location on the salt pillow.

The original mining method (1972-1993), applied high fluid pressures in the caverns under near (90-95%) lithostatic pressures, to limit the inflow of the magnesium salts by salt creep and subsidence. Magnesium salts deform orders of magnitude faster than halite under the same stress and temperature conditions. An oil blanket was used to allow solution mining in strips, for controlling the shape of cavern and the direction of solution mining as good as practically possible. This method led to considerable losses of diesel towards updip pockets, especially in the bischofite and Zechstein 2b/3b carnallite layers, due to the irregular layering of the Mg-salts and the dipping structure on the flank of the salt pillow. Salt dissolution at some tens of metres from the injection point requires density flow for the change-out of concentrated brine by diluted brine. Diluted (and lower density) brine hence has the tendency to flow updip, hence dissolving most salt updip from the injection point and little salt downdip the structure. During about 20 years about 40 000 m^3 diesel oil was trapped in (most likely) updip parts of the caverns, most likely in smaller volumes ranging from ten to at most hundreds of m^3 each, although it cannot be fully excluded that some larger pockets merged in time.

Starting 1993 (as experiments with 2 caverns) and 1995 (for all caverns) a different way of solution mining was selected at which the brine pressures were lowered and the oil blanket was no longer required. Only for the onset of new caverns (only TR-9 since then) an oil blanket was used. As soon as sufficient salt has been dissolved to allow water to mix with concentrated brine and sufficient surface area of bischofite is available to keep the cavern brine concentrated, at sufficient distance (10-20 m) from the injection point, the water-brine mix near the injection point can no longer dissolve halite. Hence the halite itself is used as a blanket for solution mining instead of diesel. Only for start-up caverns, diesel is still required to create an initial volume.

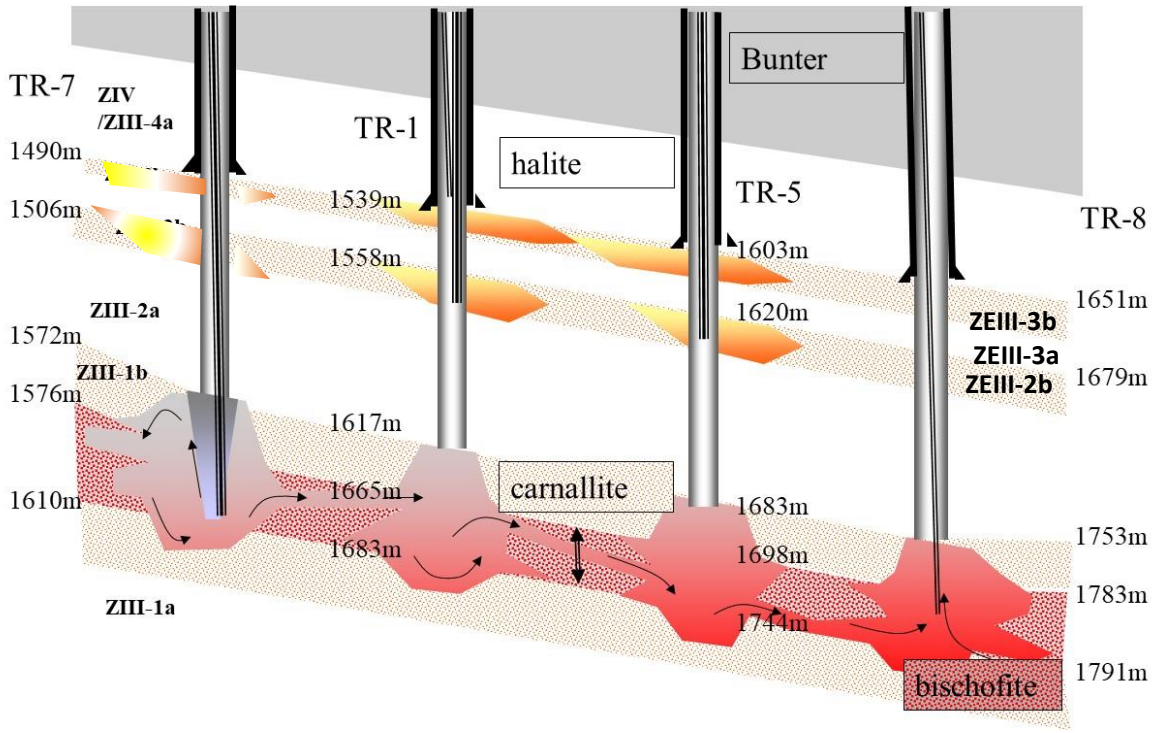

Figure 3: Drawing cross section of interconnected caverns.

Due to the pressure reduction in the cavern, salt (mainly bischofite) flowed towards the caverns, rendering additional brine production (due to the diminished cavern volume). This process is generally called cavern convergence or squeeze. The inflow of salt also allowed renewed solution mining of the bischofite, now that the salt flowed towards the production wells. The ratio of production volume to injection volume changed from roughly 1:1 before 1993 to 2:1 past 1995. From 1995 to 2018 injection and production occurred via a changing set of wells, where most caverns started interconnecting, by dissolving (at least part of) the bischofite layer in-between the wells, which were spaced at about 350-500 metres from each-other. A cross-section drawing of the interconnected caverns is given in Figure 3.

The connected total brine volume of the large cavern cluster, (TR-1 to TR-8 and VE-4), based on a mass balance, was estimated to be about 7.5 million m^3 at the start of 2018. Of this volume about 2.5 million m^3 is considered to be brine in the bischofite section that can be squeezed out at brine-hydrostatic cavern pressure within 10-15 years. The other 5 million m^3 is present within precipitates or in the carnallite section (ZE-III 2b/3b) that does not converge easily and will only be partially recoverable with decades of low pressure. Wells/caverns VE-1 to VE-3 and TR-9 are not connected. The subsidence due to the cavern convergence amounted to 1.5 cm per year, amounting to 44 cm (with respect to 1977) at the start of April 2018.

The pressure in the cavern cluster had gradually increased again in the years after 2008 (by a decreased production-injection ratio) for multiple practical reasons from about 8 MPa beneath lithostatic (75% of lithostatic) to 5 MPa beneath lithostatic (85% of lithostatic) when (on April 20, 2018) an assumed hydrofracture created a connection to the overburden, expelling about 100,000 m^3 of brine with a pressure drop of about 3 MPa in the cavern system, according to Nedmag's best estimate (Fokker, July 2018). After the event (and within an estimated 1-2 weeks), the fracture closed and leak-off stopped or was decreased to volumes that are too small to detect. The background of the leakage and ways to prevent future leakages in the present cavern cluster, non-connected caverns and new caverns are the topic of this document.

1.1 Short summary of Leakage incident.

On the 20th of April 2018 a pressure loss of about 1 MPa was noticed in the cavern field in about 3 minutes at three wells (TR-1, TR-2, TR-5). After about 30 minutes also the other wells in the cavern cluster had dropped in pressure to about this 1 MPa. During the subsequent two days the pressure in all wells of the cluster dropped further to a total of about 3 MPa, where after the pressure seemed to stabilize.

At first a casing problem was expected (Figure 4), where brine could have leaked into the overburden. Well TR-2 was inspected in the weeks thereafter. This casing does not contain any tubings anymore, so the casing wall could be inspected with cameras and wall thickness measuring tools. No damage was observed. Wells TR-1 and TR-5 were inspected from within the injection tubings, which did not allow proper inspection of the casing itself. However, no changes were observed with respect to earlier surveys. Computations of flow capacity of a 10 ¾" casing showed that the computed early leak-off (estimated at about 25,000 m^3 during the first 30 minutes) could have never flowed through a single casing, not even through all 3 casings.

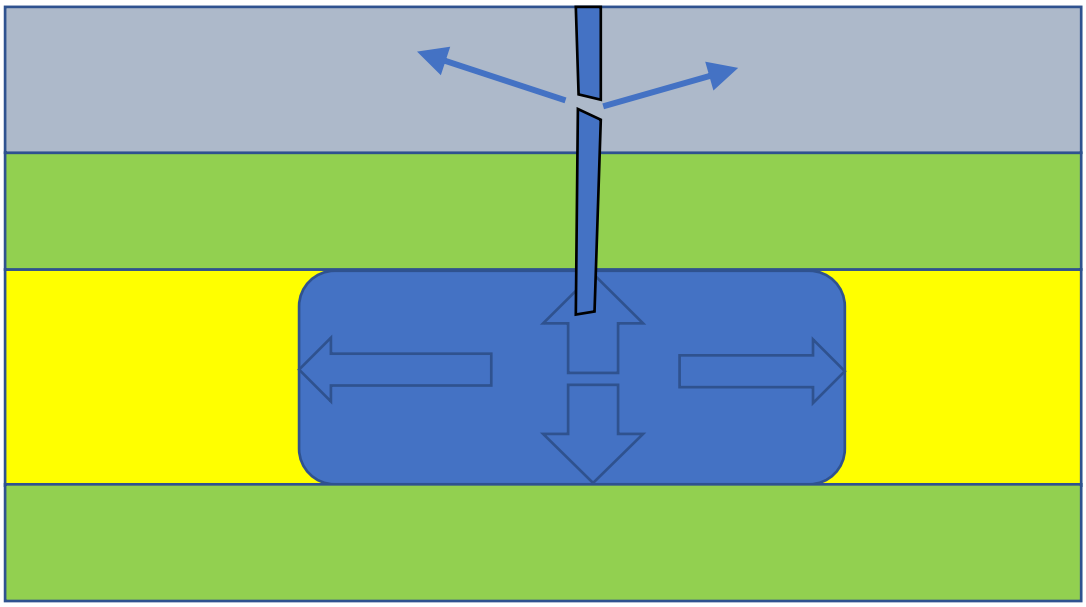

Fig. 4 Casing failure (shear or tension) and fluid flow (blow out) via a breach

A hydrofracture, Figure 5, became more likely as the root cause, but the common belief was that hydrofractures could only occur at pressure levels very near or above the lithostatic stress level, a stress level confirmed by the Leak Off Tests of the casing shoes while drilling in 1982-1990.

Excluding casing damage as a cause for leakage, the only other alternative to hydrofracturing is a complete roof-fall (Figure 6), where salt blocks fall into the cavern as a result of dilatant disintegration (also called tertiary creep). Partial roof falls are not uncommon in salt mining as an effect of spalling due to hard layered inclusions (Figure 7), such as anhydrite banks. This usually leads to casing damage, but not to leakage via the salt. A complete salt-roof fall (over the full 100 metres height) would most likely damage casings and would most likely lead to a cavern pressure drop towards fluid pressure levels of the deeper overburden (about 1.15 sg or 17 MPa at 1500 m depth) and not stabilise at about 24 MPa, which hints at a (near) closure of the leak path, that is unlikely after a roof-fall.

Between May and November 2018, the fluid pressures in the cluster are maintained at a level that prevents reopening of the fracture and the pressure development is in alignment with the theoretical pressures required to squeeze the amount of brine to surface. Water injection (other than for dilution and occasional flushing) has stopped, and for 2018 and 2019 it is expected that cavern convergence only can bring sufficient brine to surface so that water injection is not required to support pressures. Short shut-in cycles show a pressure increase that is in line with the cavern-cluster stiffness (brine and salt) of about 25.000 m^3 per MPa, identical to the value derived from pressure cycles in the period 2010-2018. Subsidence bowl volume estimates, using INSAR monthly averages, assisted by well-site GPS height measurements, also indicate the the bowl volume augmentation is line with the production volumes (and derived convergence volumes). It is expected from data-analyses that leakage stopped already end of April to early May 2018 and that about 100,000 m^3 was leaked-off into the overburden, of which 75.000 m^3 in the first two days.

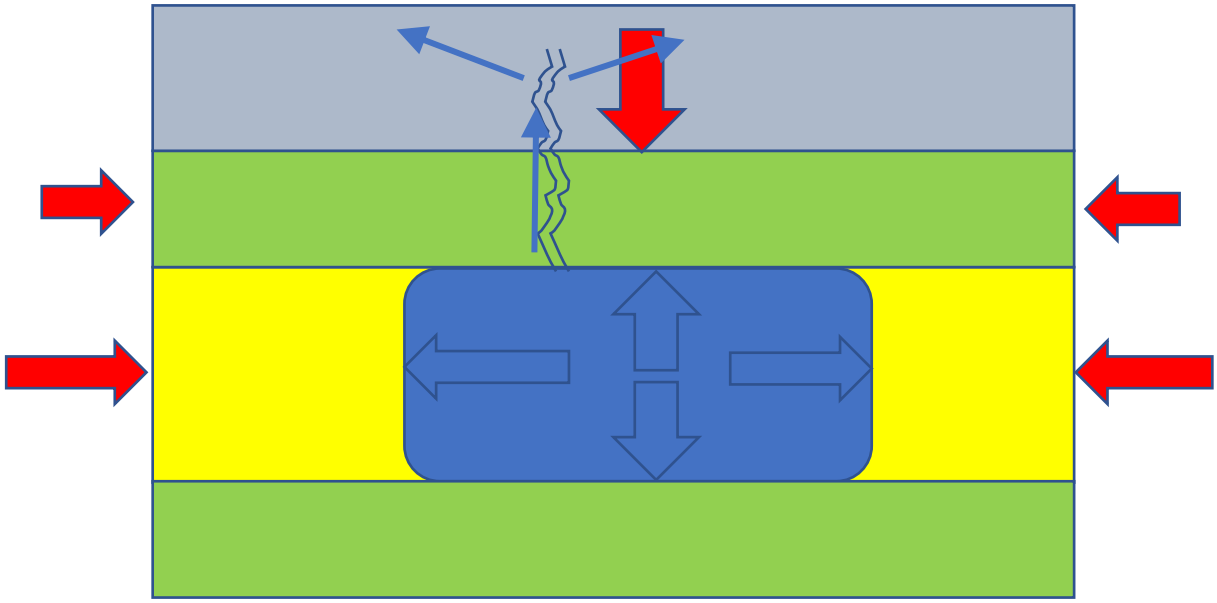

Fig. 5: Hydrofracture at a fluid pressure level that exceeds the salt stresses in the cavern roof.

.

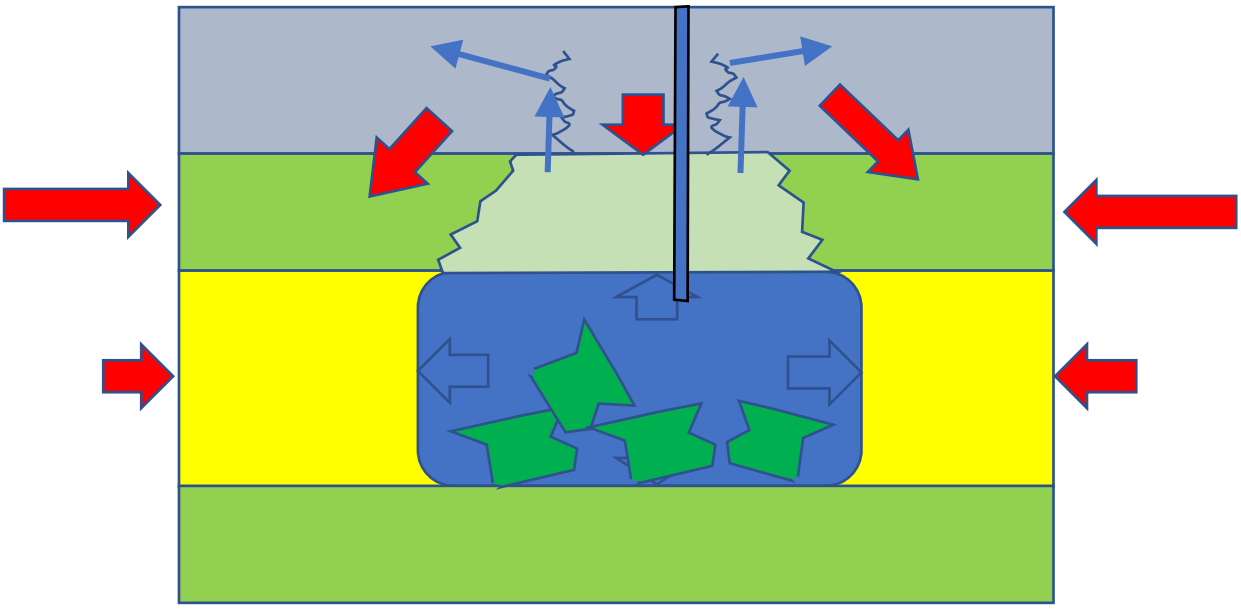

Fig 6: Complete rooffall, connecting the cavern with a permeable (or more easy to fracture) overburden

Other studies have focussed on the brine migration path, potentially carrying some former blanket oil (diesel). The brine most likely fractured the Buntsandstone and ended somewhere in the Vlieland sands (base Createous at about 1100 m depth). The fracture potentially developed further upwards towards the Upper Cretateous chalk (with an arrest around top chalk at ca. 400 m depth). No pollution with brine or oil was observed in shallow to medium deep monitoring wells or water wells. Also the casing shoe of the TR-2 16” surface casing (at 402 m in top Chalk) can be sampled and does not give indications of oil or magnesium chloride brine. If magnesium chloride brine did penetrate into the Chalk, it most likely flowed into the lower region, given its high density with respect to formation brine density at the top Chalk (about 1.1 kg/l, NaCl brine).

The following chapters will focus on ways to prevent leakage during future solution mining (in the cluster, the standalone- and new caverns). Other reports will deal with the effects of future leakages in the form of fluid permeation through the salt roof post-abandonment. Chapter 5 will focus on the potential post-abandonment leakage via fractures.

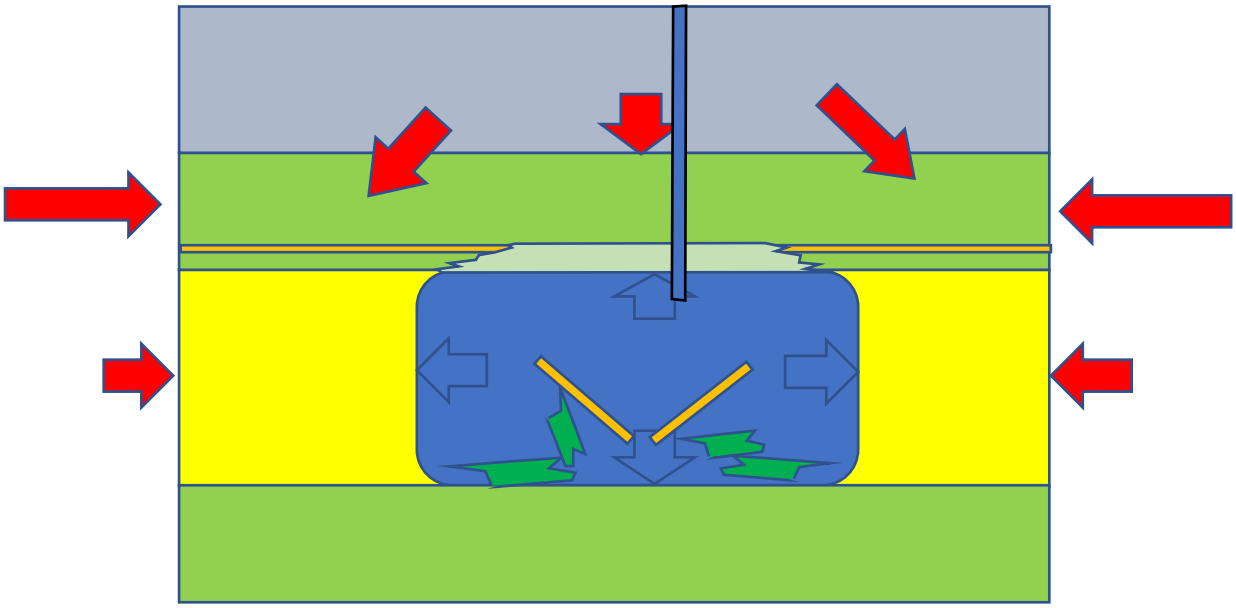

Fig 7 Partial rooffall, due to spalling effects of a hard elastic inclusion (anhydrite) in the cavern roof. This mechanism will not lead to leakage, but most likely does lead to casing damage.

2 Analysis of cavern roof integrity–axisymmetric analysis

As a result of two decades of low brine pressure in the Veendam cavern cluster, non-dissolved magnesium salts were squeezed out and thinned by about 1 metre. The surface subsidence was about 44 cm early April 2018. In order to understand the principle of stress redistribution, and still have a fast method of modelling and computation in May and June 2018 an axisymmetric mesh was chosen to represent the Nedmag cavern cluster. For forward modelling and to compute the interaction of the cluster with the non-connected caverns, also a 3D modelling effort was performed in the months thereafter, to be discussed in chapter 3.

The rock deformation was modelled using an axi-symmetric approach, assuming a single large cavern representing the central caverns TR-1-2-5-6 in the middle as a 600 m diameter (300 m radius) cavern, flanked by wing caverns (TR-3-4-7-8-9, VE-4) in the vicinity, represented by a ring cavern in the axisymmetric approach with a radial span of 200 m. This supplies a support of magnesium salts even within the area of the cavern cluster. Without its presence the cavern system would have created a much larger subsidence from elastic perspective only. The mesh is depicted in Figure 8. Details of the magnesium salt interbedding were left out in this approach, assuming the ZE-III-1b/2a/2b/3a/3b salts to form one single formation and one single cavern. The purpose was to compute stresses in the salt caprock and the overburden, which are closely related to the deformation in the overburden.

The most important salt creep parameters are the bischofite parameters, as main driver for cavern convergence, and the halite creep parameters in the cavern roof (ZE-IV halite), that drive the stress relaxation in the roof. Steady state power-law creep is (when integrating a temperature dependence in the pre-exponent) usually written in a the form of a (Von Mises) strain rate dependence on the Von Mises shear stress to the power m. The Von Mises strain translates to the axial strain of a triaxial loading test and the Von Mises stress translates to the differential stress (axial minus radial) of a triaxial loading test.

$$\dot{\varepsilon}_{VM} = A\sigma_{VM}^{m}$$

The bischofite creep parameters are approximately known from the thesis of Urai (1983) and show (for low shear stresses) a power law creep behavior with a power *m* of 1.6-2.0. The halite creep parameters for the ZE-IV salt have not been tested for long term creep behavior. In the thesis of Fokker (1995), using clean halite salt from the ZE-III-2a formation, steady state creep at 70 °C could not be reached in a period of weeks (practical test limit). For differential stresses of 15 MPa, this means that the steady state creep rate would have been below 1 10^{-9} /s (3% per year). Assuming a power *m* of 4 (most halite test results worldwide indicate powers ranging between 3.5 and 4.5), this would lead to a creep rate of less than 2 10^{-14} /s at a differential stress of 1 MPa. A pre-exponent *A* of 1 10^{-14} /s has been taken as best guess parameter. For the ZE-II salts, that are known to creep an order of magnitude faster than ZE-III, a value of 1 10^{-13} /s has been adopted, also taking the slightly higher temperature (80-100 °C) into account for the deeper salts.

The magnesium salt power has been taken from Urai and assumed to be 2 in this axisymmetric simulation (more or less averaging the bischofite power with the higher power in carnallite and halite) and 1.6 for the 3D computations, where the ZE-III-1b formation is modelled separately. The pre-exponents have been fitted by comparing modelled and measured subsidence rates, since the bischofite is not present as a pure layer, but intermixed with other salts. The pre-exponent should be (and is) lower than the values obtained for pure bischofite.

.

The stiffness of the Buntsandstone overburden has been taken from sonic data from the Nedmag wells, rendering a dynamic stiffness of about 20 MPa. Correlation gives a static stiffness (Young's Modulus) of 5-15 GPa, where 12 GPa has been chosen (to provide the best subsidence fit to measurements). The shallow overburden stiffness (Cretaceous) has been given an estimated stiffness of 5 GPa, whereas the shallow overburden has been given an average stiffness of 0.5 GPa. The 3D approach allows a bit more variation in parameters. The pressure history is shown in Figure 9, where the limited 1985-1995 squeeze is simplified by assuming a pressure drop starting 1990.

In the axisymmetric analyses all the magnesium bearing layers (ZE-III-1b/2b/3b) and the intermediate halite layers (ZE-III-2a-3a) have been assumed to form one layer. The analysis does not allow cavern to cavern details anyway. This is the yellow layer in Figure 8.

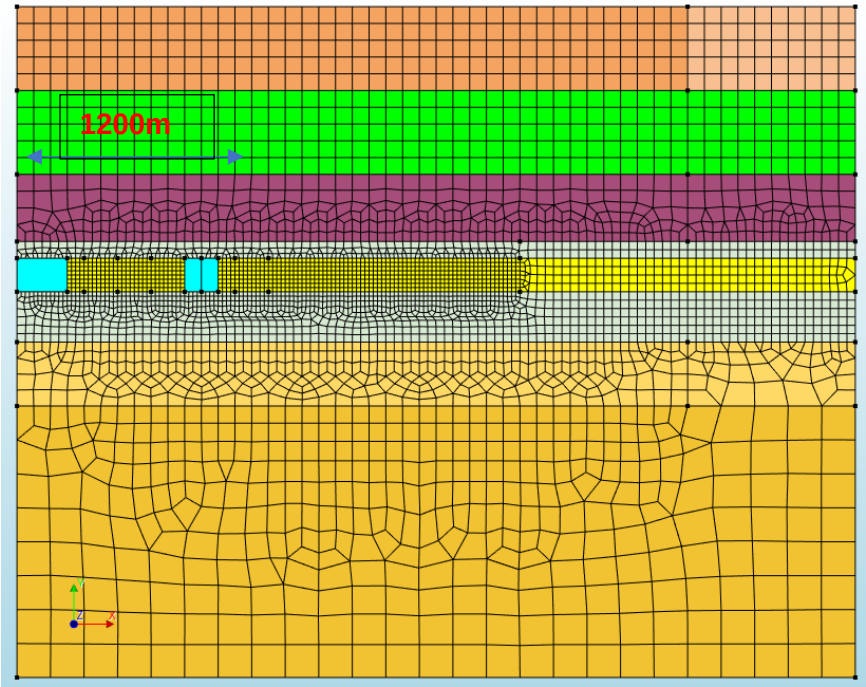

Figure 8: Mesh and geology. The yellow layer represents the combined magnesium containing layers. The gray layers are the ZE-III1a and ZE-IV halite layers enclosing these Mg-salts. The purple layer is the Buntsandstone, the green layer the Cretateous and the top layer the North Sea Group.

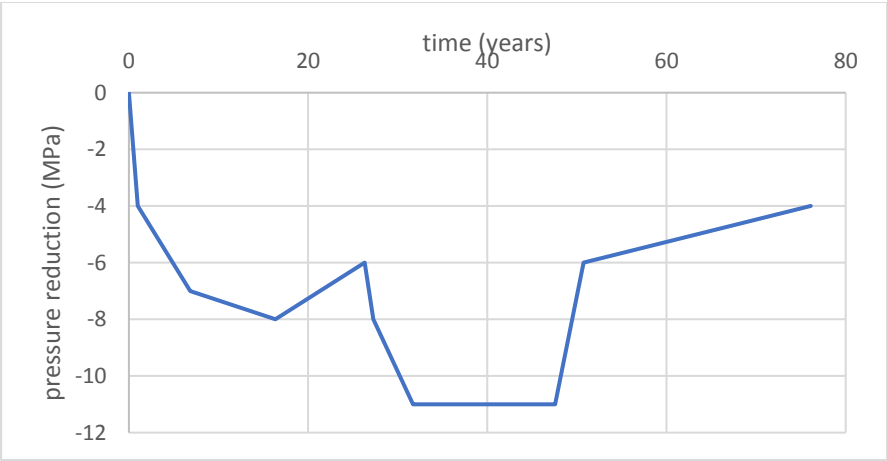

Figure 9: Pressure loading of salt caverns in time. The pressure reduction is modelled from 1990, where in 2018 the pressure drop occurred to 8 MPa below lithostatic, presumably dropping to 11 MPa somewhere in 2021 (year 31) and kept constant for 16 years.

Figure 10 shows the vertical deformation in April 2018, amounting to some 44 cm at the heart of the bowl (top-left). When subsidence is plotted for measured subsidence by levelling, but scaled to 40 cm in the middle, the resemblance is very good, see Figure 11.
The shape of the (2016) subsidence bowl, such as determined by SGS-Horizon with a Geertsma-Van-Opstal analysis (with fluctuating rigid base), with a fixed centre at cavern (casing shoe) TR-1 is plotted as red dots and compared with the levelling data (grey dots). Superimposed are the computed bowl by Finite Element analysis (red line). For reference also two alternate computations have been plotted. Plotted are case where the deformation is all elastic (and subsidence is scaled to 40 cm subsidence) as blue line and a case where the pressure reduction only occurred in the central cavern, also scaled to 40 cm (yellow line). Also a Gauss fit has been plotted through the bowl, also showing a similar good fit. The Gaussian fit can be written as:

$$w_r = w_0 \exp(-\chi r^n)$$

with w_r the subsidence at radius r (in meters), w_0 the maximum subsidence (r=0), with χ and n fitting parameters. The displayed fit parameters are χ=3 10^{-6} and n=1.7.

The sharp bowl from the central cavern only can be fitted with χ=4.5 10^{-6} (and n=1.7),

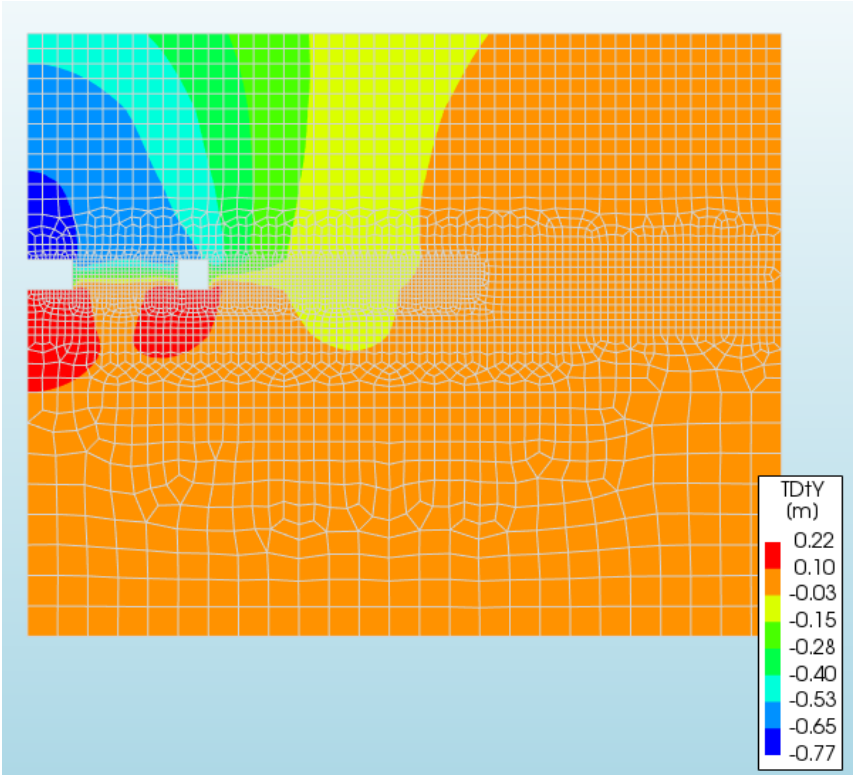

Figure 10: Vertical deformation (subsidence at top of about 44 cm) around early April 2018.

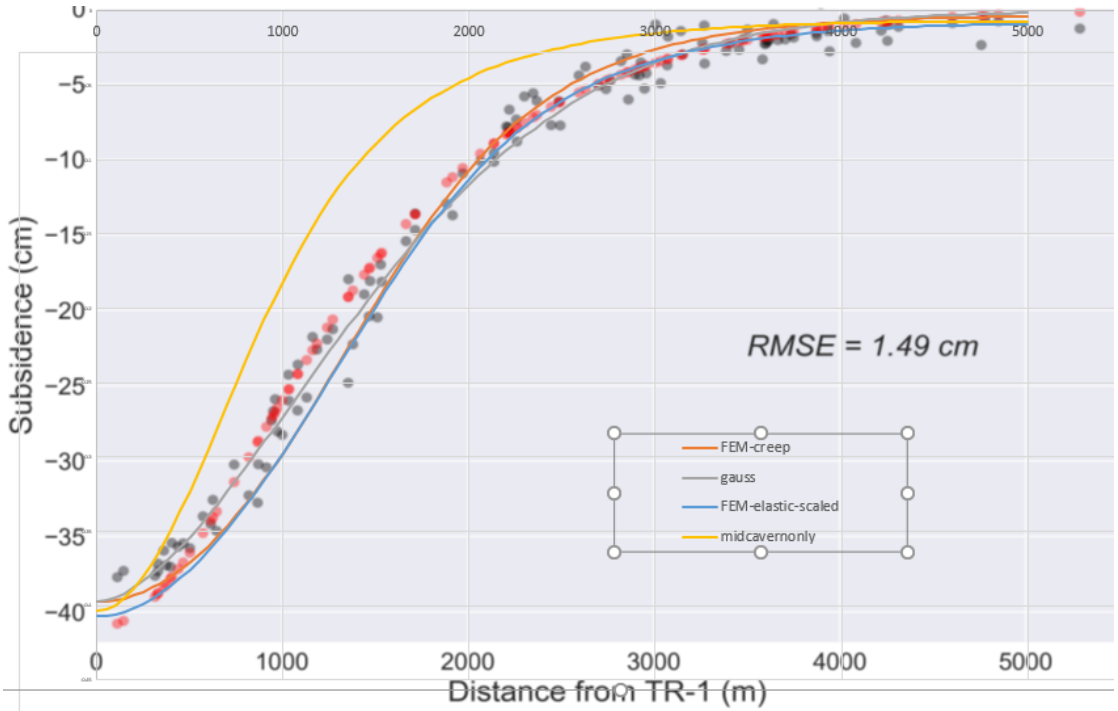

Figure 11: Comparison of the levelling- measured and computed subsidence bowls, scaled to 40 cm in the bowl centre. Blue line; this axisymmetric study. Grey dots: levelling data 2016. Grey line: best Gauss fit. Red Dots: SGS-Horizon fitting using with Geertsma-Van-Opstal (with time dependent rigid base). The yellow line is the theoretical bowl shape for convergence from the central cavern section only (for reference).

.

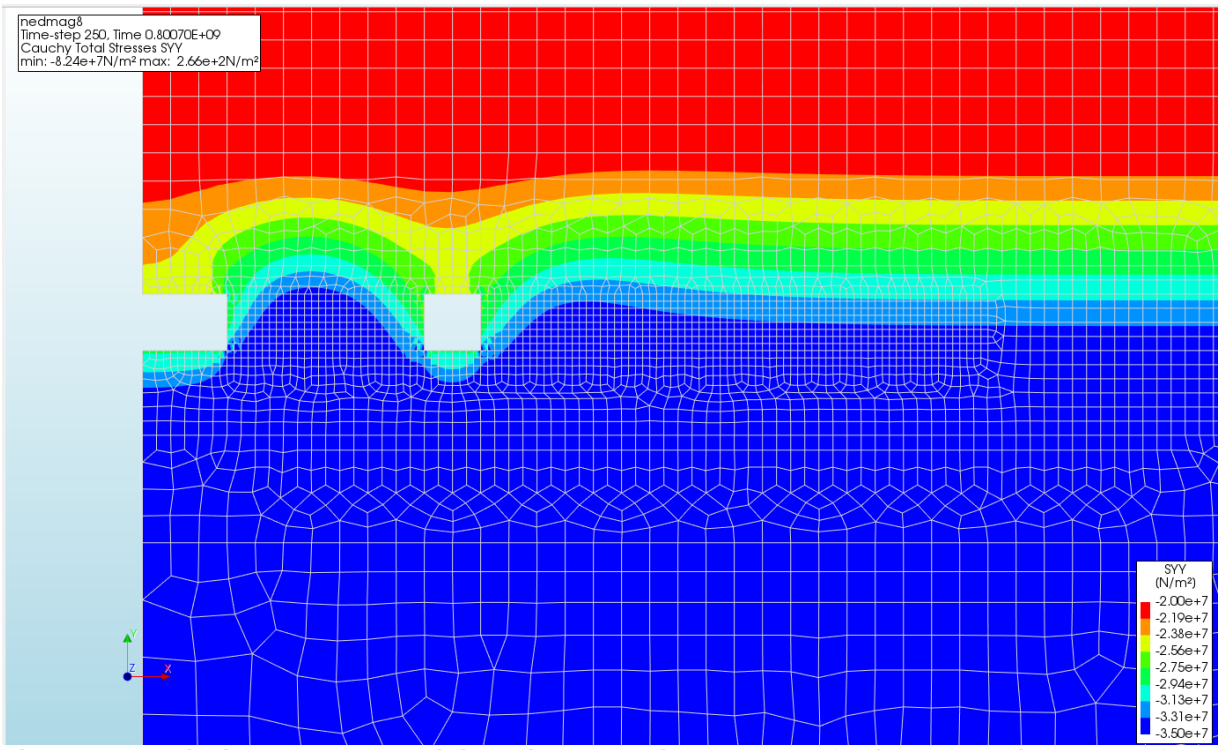

Figure 12: vertical stresses around the salt caverns by 25 years of salt creep and 44 cm surface subsidence. The colour bar ranges 20-35 MPa (2-3.5 10^7 N/m^2). The stress reduction around the central cavern is about 5 MPa.

Analysis shows that by the prolonged sub-lithostatic pressure and the overburden deformation, by April 2018, the salt stresses in the cavern roof (in all directions) have decreased by some 5 MPa ($0.5\ 10^7$ N/m^2). The main driver seems to be the arching of stresses due to cavern convergence and subsidence, where the vertical stresses in the Buntsandstone decreased by about 5 MPa too. The vertical, horizontal and minimum principal stresses have been plotted in Figures 12 to 14.

The creep parameters of the halite roof seem less critical, provided they allow at least 0.5% creep to allow the salt stresses to get into a more isotropic stress state during the low pressure period. An analysis with a hundredfold faster halite creep under similar stress conditions (A=1 10^{-12} /s instead of A=1 10^{-14} /s) showed a very similar result (Fig 15), with only slightly lower minimum stress levels in the order of 6 MPa sublithostatic.

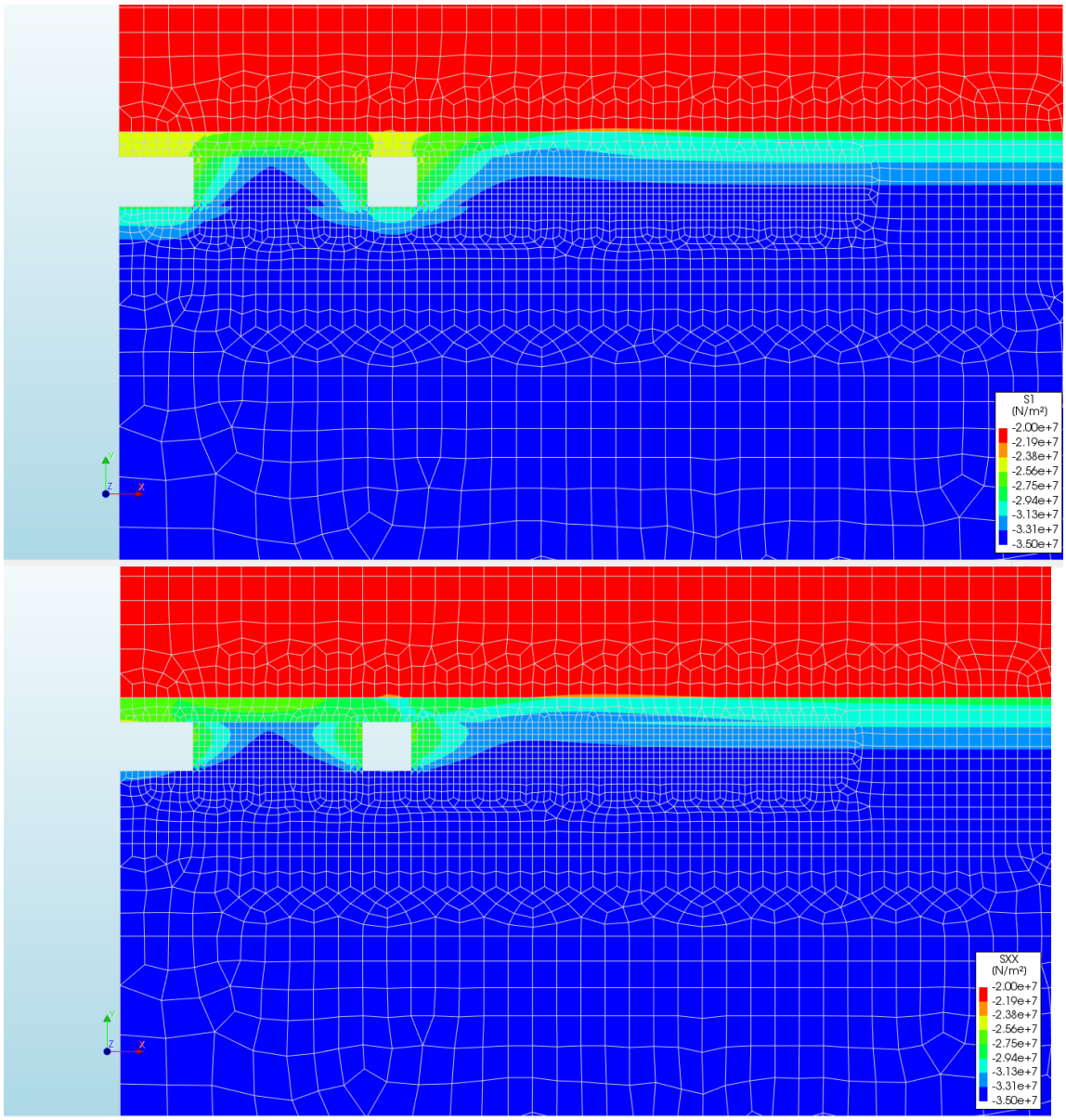

Figure 13 a/b: minimal (top) and horizontal (base) stresses above the salt caverns by 25 years of salt creep and 42 cm surface subsidence. The colour bar ranges 20-35 MPa. The stress reduction around the central cavern is about 5 MPa. The minimum stress in the salt above the caverns is the vertical stress and almost equal to the brine pressure.

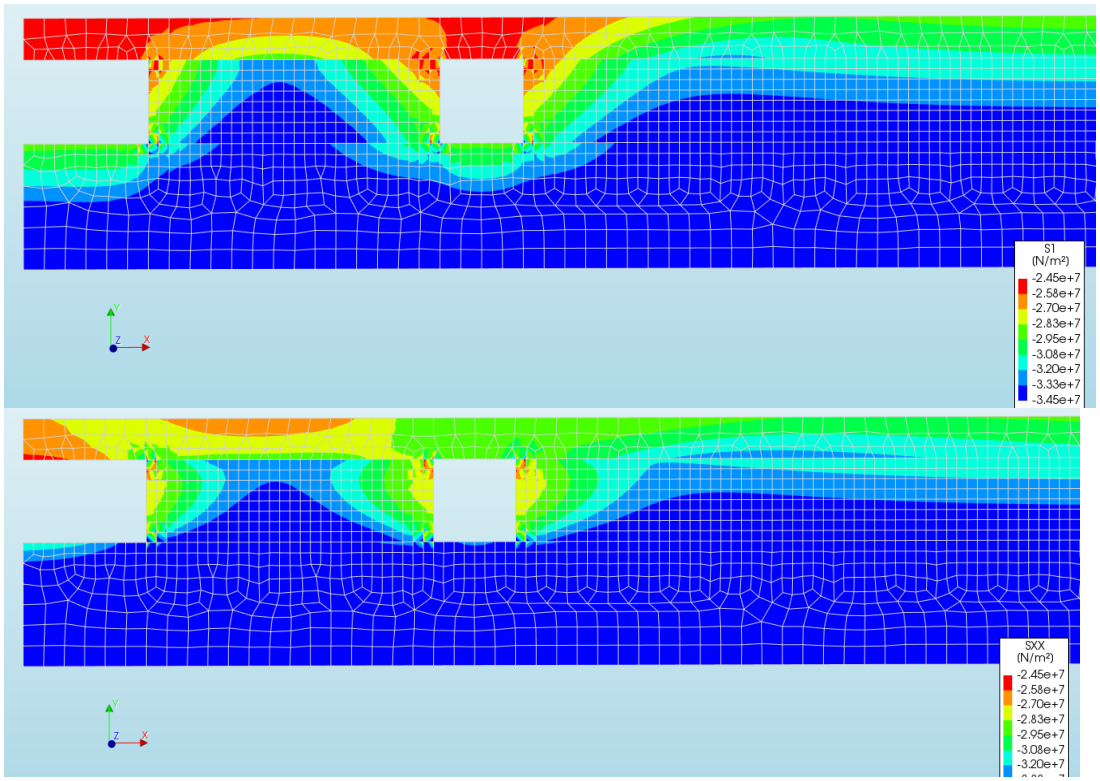

Figure 14 a/b: minimum (upper) and horizontal (lower) stress in the salts by 25 year creep and surface subsidence. The colour bar runs from 24.5 to 34.5 MPa (2.5-3.5 x 10^7 N/m^2). The reduction in horizontal stress above the central cavern is about 5 MPa.

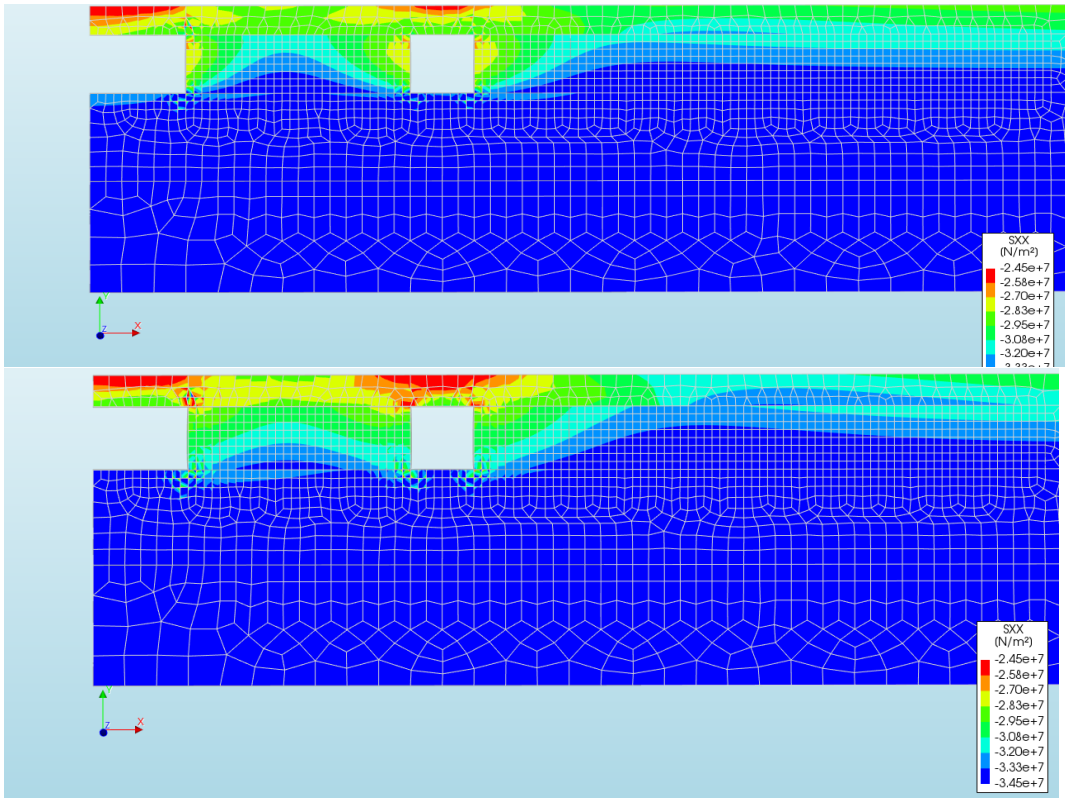

Figure 15 a/b: Horizontal stress with 100-fold faster creep for halite-ZE-III for 25 years (upper picture) and 60 years (lower picture) of cavern convergence and subsidence. The stress in the caprock above central cavern has reduced with 6 MPa in both cases.

When pressures are increased again after a period of low pressure mining, the salt stresses bounce back a little, mainly due to elastic effects (lateral contraction / Poisson effect), but creep cannot reverse the stresses at elevated fluid pressures in this case, without exceeding the fracture limit (assuming a low tensile strength of 1-2 MPa of halite). Lateral salt movement due to creep can increase the horizontal stresses at constant brine pressure, but computations show that this process is negligible in case the cavern extent (diameter) is larger than the thickness of the salt, like it is assumed here (with a 600 m diameter cavern cluster and a 100 m roof thickness). Also for the ring cavern of a span (in radial direction) of only 200m the same still holds true, although here the stress reduction in the salt roof is somewhat less (3 MPa).

The Von Mises stresses (differential stress for a triaxial test circumstance) are plotted in Figures 16 and 17 for the 2018 (8 MPa sublithostatic) and 2022 (11 MPa sublithostatic) cavern pressure, indicating (for the salt) stresses of up to 5 and 10 MPa respectively, far below values where significant dilatant creep or even roof failure could be expected (20-35 MPa) for unsupported salt.

When the cavern convergence and subsidence continues, the arching effect also continues, lowering the stresses in the halite roof even further. Assuming that most of the remaining free brine in the 1b section can be squeezed out (about 3 million m^3, including non-connected caverns), and a significant part of the 2b/3b cavern sections (1-2 million m^3) a total of 4-5 million m^3 brine can be squeezed out in coming two decades. This will result in a subsidence bowl of an additional 30 to 40 cm. If we allow numerical subsidence to continue to 100 cm, while decreasing the brine pressure to the lowest possible brine pressure that still allows brine flow towards the surface, (65% of -11 MPa below- lithostatic), and we allow the cavern pressures to increase again to 80% of -6 MPa below- lithostatic) afterwards in about 1 year (assuming a preparation for final abandonment), we see that the stress reduction with respect to the original stress is, about 6 MPa, i.e. 1 MPa in excess of the 2018 stress reduction. See Figure 18 for horizontal stress levels and Figure 19 for the associated subsidence.

The salts in the cavern roof and the walls have a reduced level of minimum stress with regard to the original lithostatic stress level. The effect is however only stretching to about 300 metres distance from the cavern wall (the far end of bischofite dissolution). Caverns that are located beyond this 300 m and that have not experienced low brine pressures for a decade or more themselves, will not see the lowered fracture pressure. Wells such as TR-9 or the projected wells VE-5 until VE-8 are all beyond this level of 300 m even with conservative assumptions on the leaching front from the cluster cavern complex. A better reference to these wells is given in the 3D numerical approach in Chapter 3.

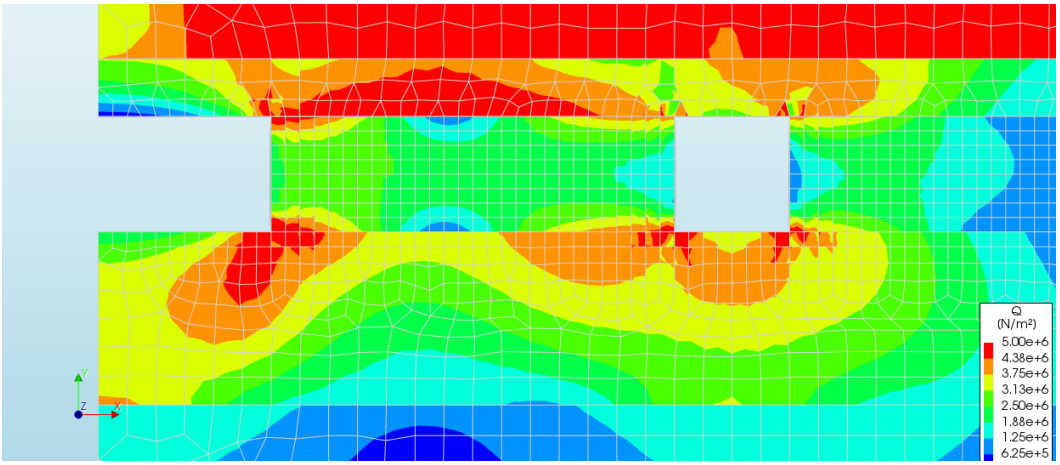

Figure 16: Von Mises stresses in salt layers (and Buntsandstone) at 8 MPa sublithostatic pressure. Within the salt the largest Von Mises stresses are around 5 MPa, considerably lower the values at which dilatancy or collapse could occur (20-35 MPa).

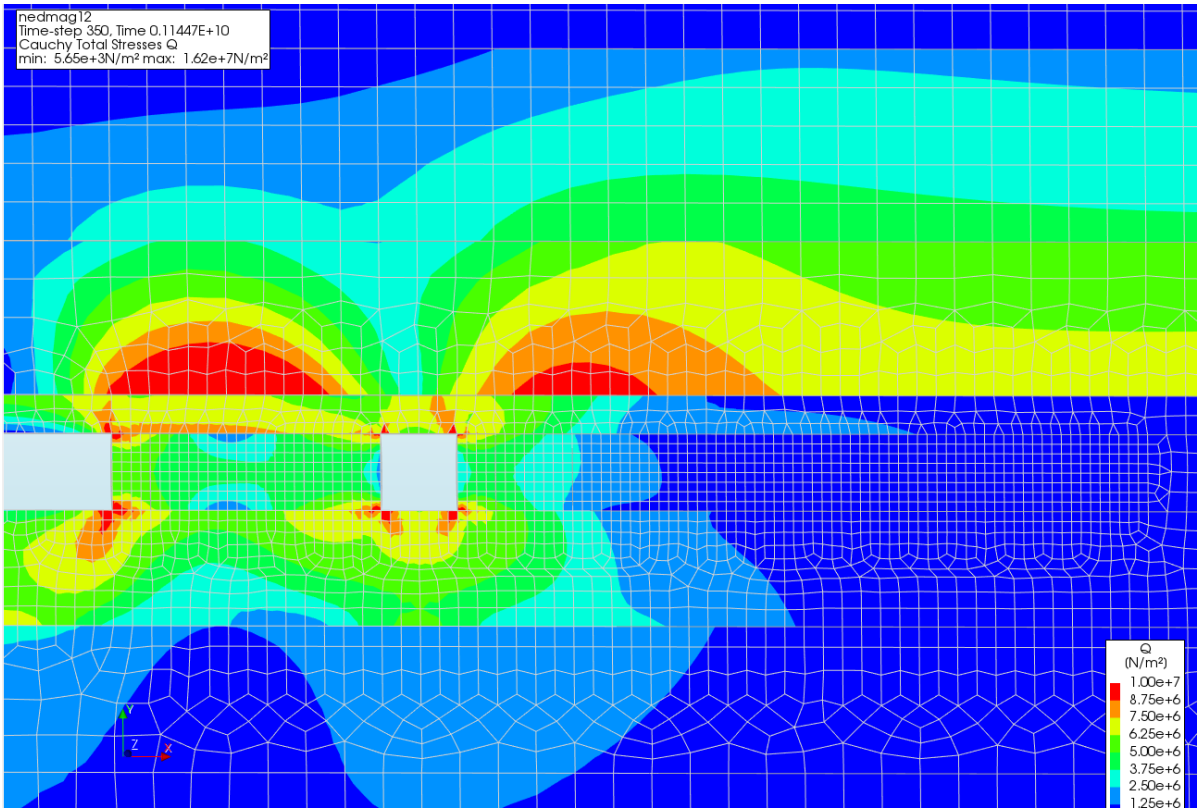

Figure 17: Von Mises stresses in salt layers (and Buntsandstone) at 11 MPa sublithostatic pressure. Within the salt the largest Von Mises stresses are around 10 MPa in the artificial corners of the model, considerably lower the values at which dilatancy or collapse would occur (20-35 MPa).

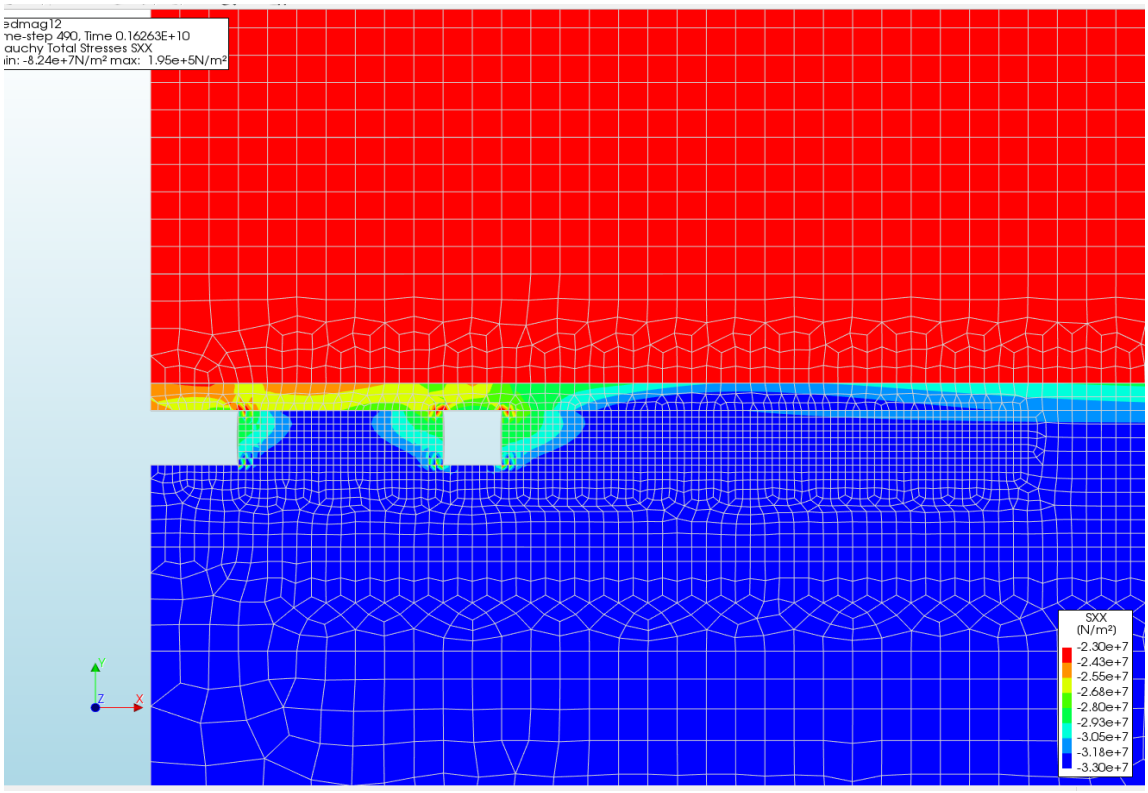

Figure 18: Horizontal stresses in salt layers (and Buntsandstone) at 6 MPa sublithostatic pressure after a prior 12 MPa sublithostatic period.

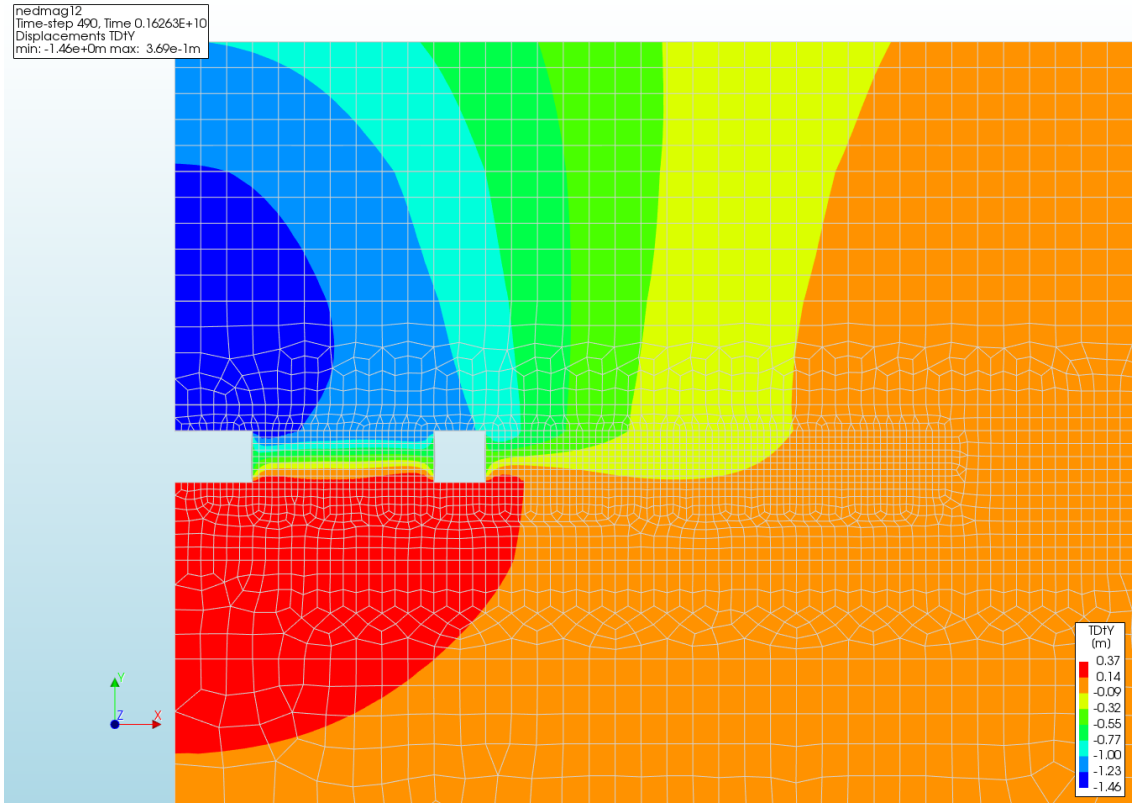

Figure 19: Modelled subsidence at the end of low pressure mining (max 1 metre in the centre), which is conservative, since the effect of precipitates is not taken into consideration, that will slow down cavern convergence in the final stages of convergence.

3 Analysis of roof stability criteria – 3D analysis

In order to assess the stress evolution for specific non-connected caverns, their mutual influence and different phases of development, a 3D model has been created for the Nedmag cavern field, including the projected cavern-sets VE5-6 and VE7-8 and the solitary caverns TR-9 and a solitary cavern representing a smaller nearby cavern like VE1-3.

In this model the horizons have been derived from a Petrel model that stems from an interpreted 3D seismic survey, depth corrected for well data. The surfaces have been reworked in SKUA-Gocad to a congruent set of triangulated surfaces. Additionally, the side surfaces for the caverns have been created to allow separating cavern fluid from salt. An area of interest has been created around the caverns that allows mesh refinement and the creation of 4 artificial surfaces in the ZE-III-1b bischofite, which force the mesher to divide the layer into at least 5 elements. Squeeze flow in a thin layer can only be modelled with any precision if the area contains at least 3-5 elements. Outside the area of interest the bischofite does not contain sublayers, hence being not very reliable for squeeze flow, but the axi-symmetric model indicates that flow is limited at 500 m from the cavern wall. The mesher resulted in about 400,000 tetrahedrons, which were given quadratic elements (10 nodes including mid-nodes) for higher accuracy.

The caverns have only been modelled as separate entities in the 1b layer, since the volume and extent are the largest here. In a future update the carnallite top caverns might be added, but since the new caverns (and latest cavern TR-9) will not have a solution mining volume here, this has been neglected in this model as the study is focused on solution mining in the future in the non-cluster wells and the setting of safe pressure limits.

The cavern shape of the cavern cluster has been estimated from the casing shoe locations and experience from the leakage-incident and the axi-symmetric modelling, assuming a central part in the shape of a ham and some connected and non-connected areas. The exact location of the brine volumes is not known. What is known, is that solution mining cannot happen downhill (due to the required density flow) and the connectivity of the caverns. The resulting modelled subsidence bowl is a last check on the aptness of the assumptions. Figure 20 shows the full mesh in side view. Figure 21 shows the top of the ZE-III-1b bischofite section with depth contours and outlines of the caverns, as well as some well paths for orientation. Figure 22 shows the meshed cavern bodies in top view. Figure 23 shows the meshed caverns displayed on the ZE-III-1a salt beneath the caverns

Wells VE5-6 and wells VE7-8 have been modelled in their final volume where it is assumed the caverns VE5-6 have interconnected, like cavern set VE7-8.

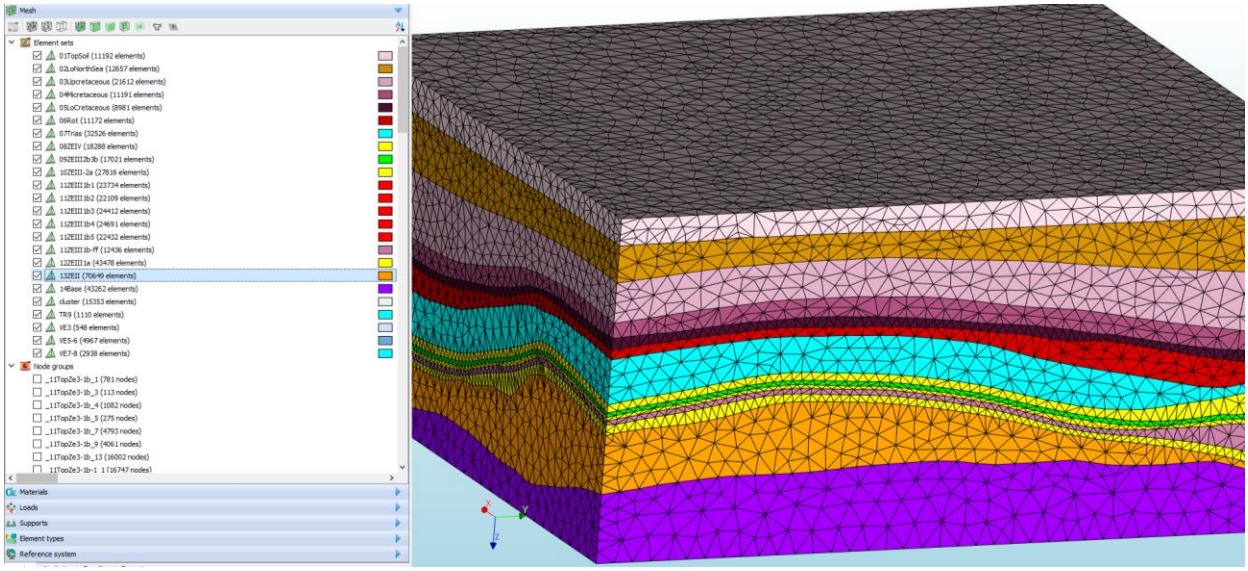

Figure 20: Formations in bird-eye view. Overburden from top to bottom: Top soil (=Upper North Sea), Lower North Sea, Upper- Mid- and Lower Cretateous, Rot, Trias (Bunter). The yellow layers are ZE-III and ZE-IV halite layers with a green carnallite (ZE-III-2b/3b) layer and maroon bischofite (ZE-III-1b) layer. The orange layer is the ZE-II salt formation and the purple is the underburden (ZE-I or Rotliegend.

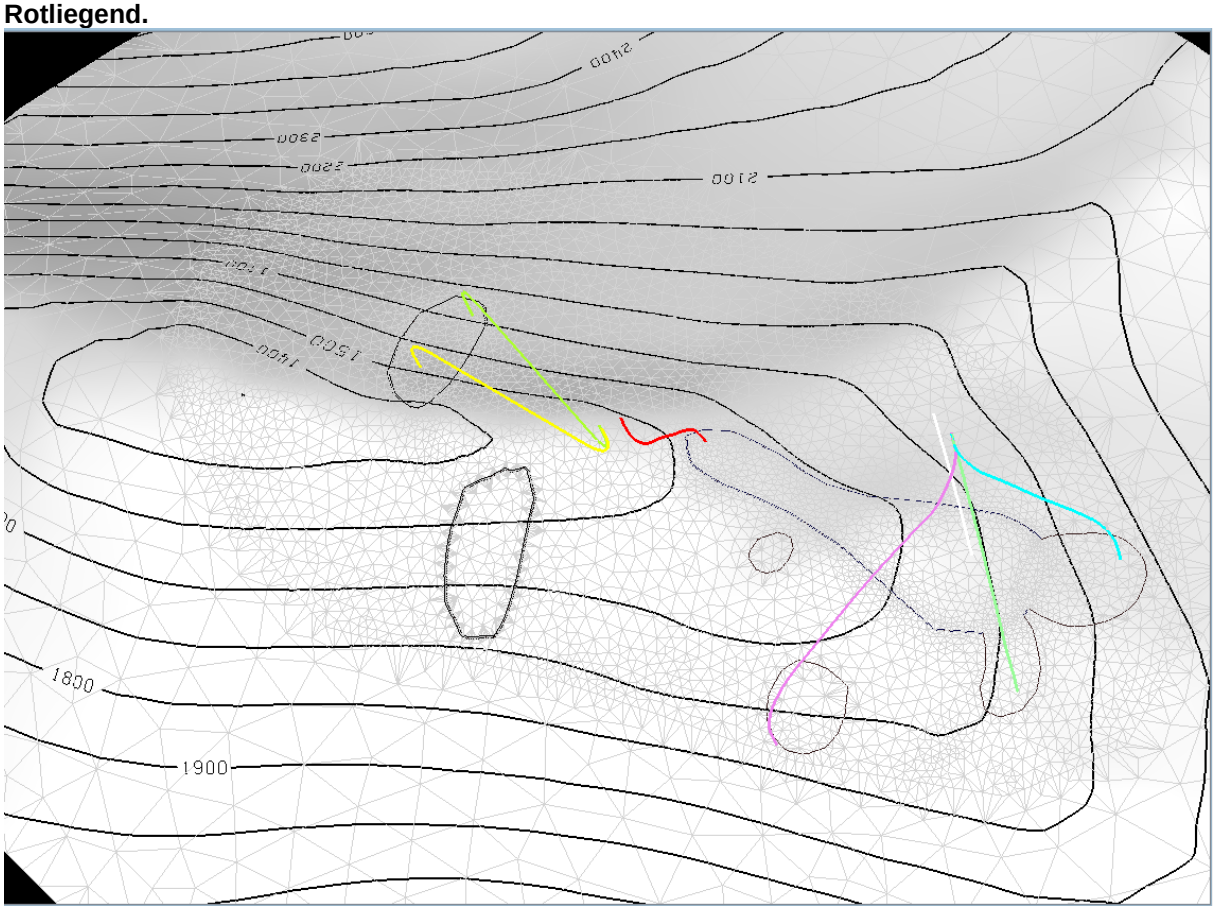

Figure 21: Top ZE-III1b with depth contour levels and outlines of the caverns and some of the well paths (red: VE-4; blue: TR4; white TR-2; green: TR-8; purple: TR-9; yellow/green: VE5-6)

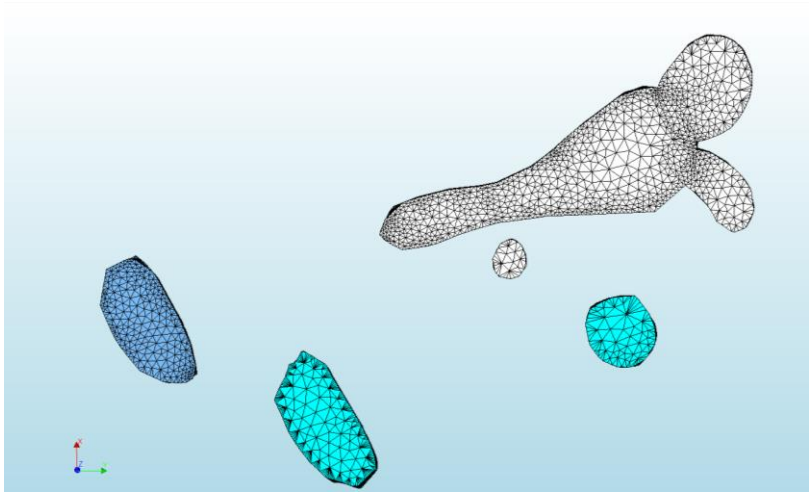

Figure 22: caverns as meshed bodies in top view.

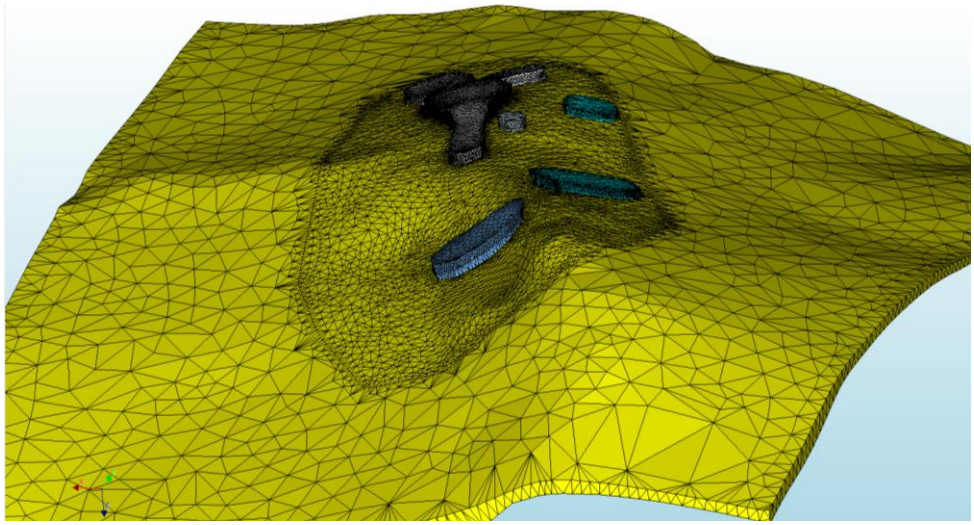

Figure 23: caverns on top of the underlying ZEIII-1a halite formation.

The cavern history has been simplified for the fact that the caverns did not have the same volume and cavern pressure over the total time of significant squeeze, starting 1993. The 2018 situation has been taken, except for the VE5-6 en VE7-8 caverns that will only exist in reality starting 2020 or later. These caverns will be modelled with having a lithostatic brine pressure for the period 1993-2020, assuming that the (artificial) influence on the remainder of the caverns and the subsidence is negligible.

The simulations have been given a similar pressure history for the cluster as in the axi-symmetric approach (but with a 12 MPa -versus 11 MPa in the axisymmetric approach sublithostatic pressure, that should be manageable for at least the deeper caverns), but allow a different pressure history for the non-communicating caverns VE1-3, TR-9, and VE5-6 / VE7-8. See Figure 24. It is assumed that all caverns will start operation under high fluid pressures and will be driven to low (brine hydrostatic) pressures as a pre-abandonment phase. TR-9 and the future caverns VE-5 to 9 have a delayed profile of pressure reduction and abandonment. After that, it is assumed that the brine pressure increases to about 93% of lithostatic due to abandonment, which is not necessarily a production strategy, but rather a check whether this would be possible without fracturing the salt roof. Prior to loading the caverns, the salt masses have been allowed to flow for 318 years (10^{10} seconds), in order to make sure that the stress initialization routines would not leave shear stresses in the salt that would lead to significant deformations in the decades of salt mining.

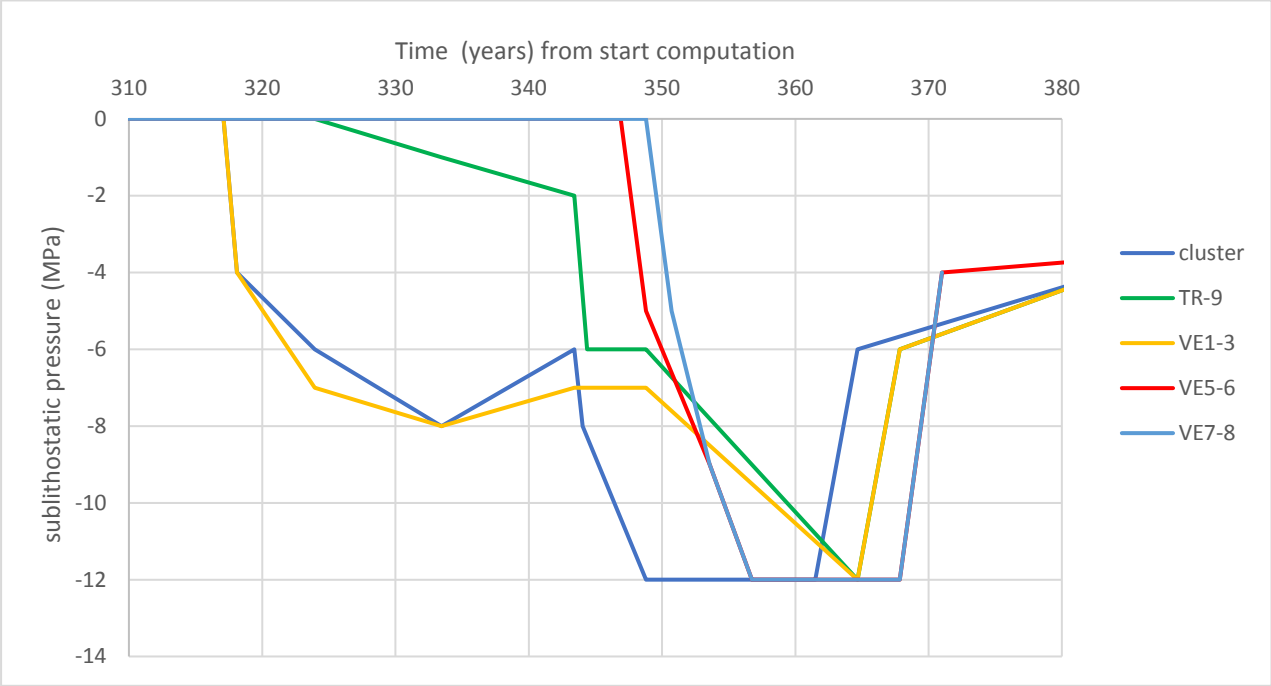

Figure 24: Fluid pressure as modelled in the Finite Element model per cavern set.

The (effective) bischofite creep parameters were history matched with subsidence. That assumes that the net amount of bischofite in the (about) 60 m ZE-III-1b is the same everywhere, where it is known that in reality the thickness varies from 5m (at the crest) tot 25 m at the flanks. Most caverns are targeted for the thickest bischofite layers nowadays. The creep around the old caverns VE-1 to VE-4 with relatively thin bischofite layers will be slightly overestimated by this averaging out of parameters. This is compensated by assuming a smaller cavern for a cavern that represents the combined effect of VE-1 until VE-3. Only VE-3 can still be mined and pressures controlled, since VE-1 and VE-2 are stripped of tubings or suspended by a cement plug respectively.

The resulting 2018 subsidence bowl is displayed in Fig. 25, which is in good alignment with the measured bowl, with a 10% contour of maximum subsidence at about 3 km from the deepest point and the 50% contour at about 1.5 km distance.

3.1 Shear stress build-up

The 2019 shear stresses (Von Mises stresses) in the cap rock (at an expected cluster pressure of 9 MPa below lithostatic) have been plotted in Fig 26. The Von Mises stresses are also plotted around 2025 in Figure 27 with an estimated 12 MPa sublithostatic level, now in combination with the effects of the new caverns VE5-6 and VE7-8. The Von Mises stress remains far below stress levels that result in dilatant failure. Also the total creep strain (Von Mises strain) remains small (< 2.5%) in the ZE-IV in the post-abandonment phase, see Figure 28. The strains in the ZE-III-2a, the (lower) cap rock for the new caverns, have been plotted in Figure 29 and are slightly higher (up to 3%) caused by some dragging effect of inward moving carnallite, even in the absence of caverns here. This effect will have some impact on the minimum stress evolution in the ZE-III-2a (which is only relevant for caverns with casing shoe in the ZE-III-2a), due to a slightly reduced stress relaxation. In absence of a man-made connection, the caverns with a casing shoe in the ZE-III-2a will keep a slightly elevated fracture gradient for a similar pressure history to caverns with a developed ZE-III-2b/3b layer.

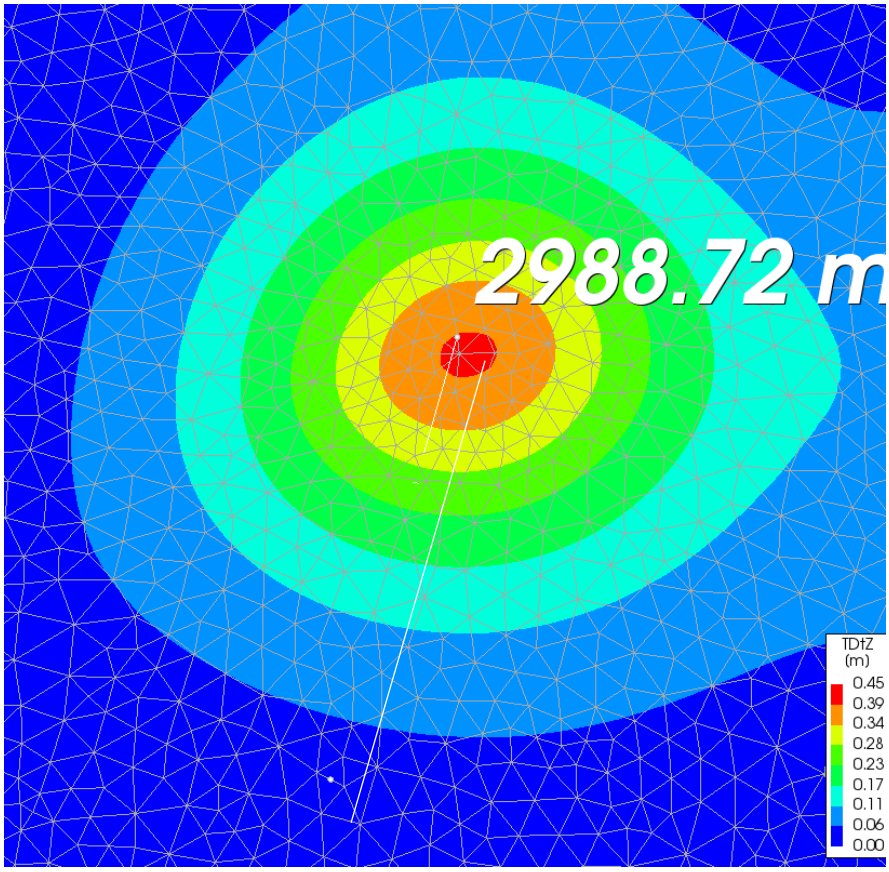

Figure 25: Subsidence 2018 with length bar to indicate the distance between the maximum subsidence and the 10% line, of about 3 km. The 50% contour is at about 1.5 km. The non-symmetric 6 and 11 cm lines are the result of boundary conditions mainly

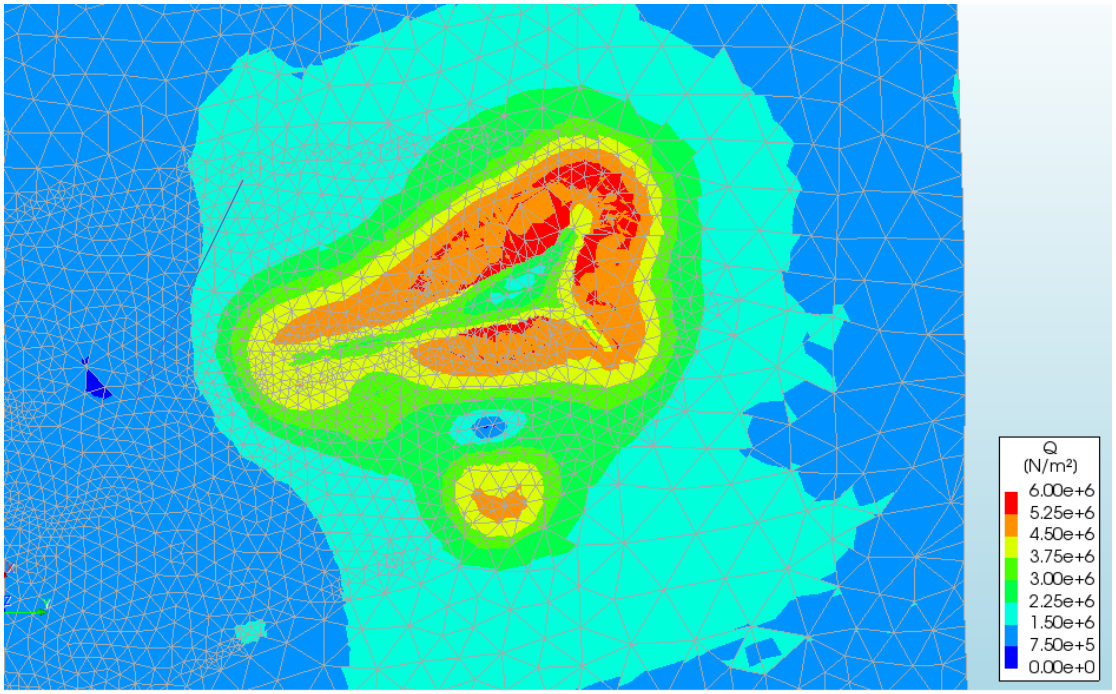

Figure 26: Von Mises stresses in the ZE-IV salt roof (0-6 MPa) at 9 MPa sublithostatic pressure in the cluster early 2019.

The low shear stresses in combination with the limited Von Mises strains, will not lead to (relevant) permeability development by dilatant (tertiary) creep in the ZE-IV halite roof. Storage caverns usually have a much more elevated shear stress development where most (or all) do not develop a (measurable) leakage path through the salt in the absence of major roof falls.

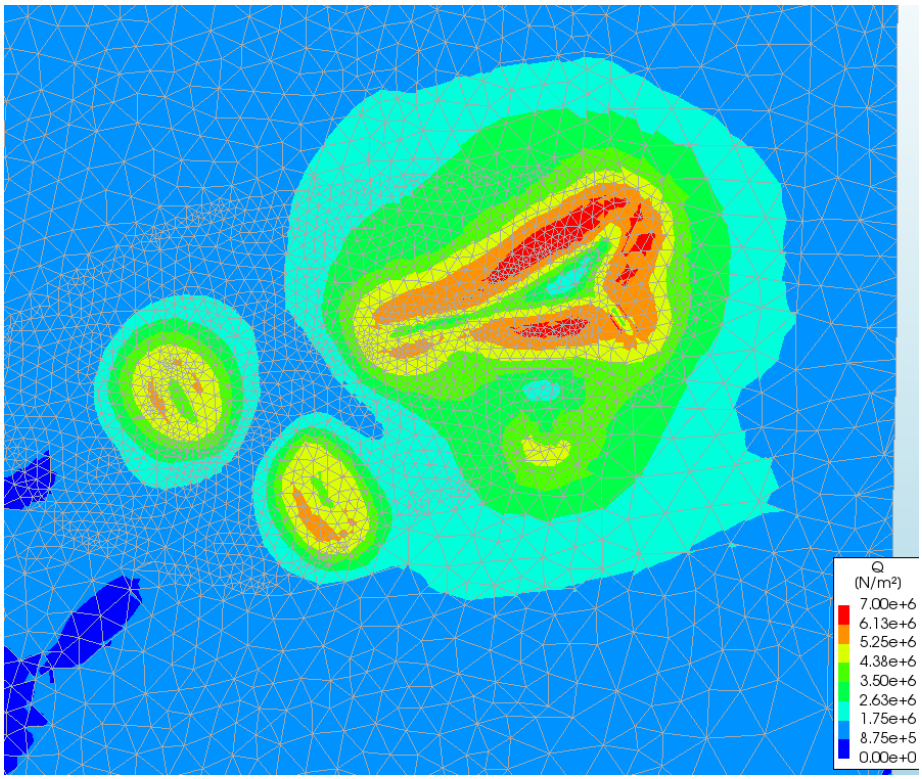

Figure 27: Von Mises stresses in the ZE-IV salt roof (0-7 MPa) at 12 MPa sublithostatic pressure in the cluster 2025 and 8 MPa in the caverns VE5-6 and VE7-8.

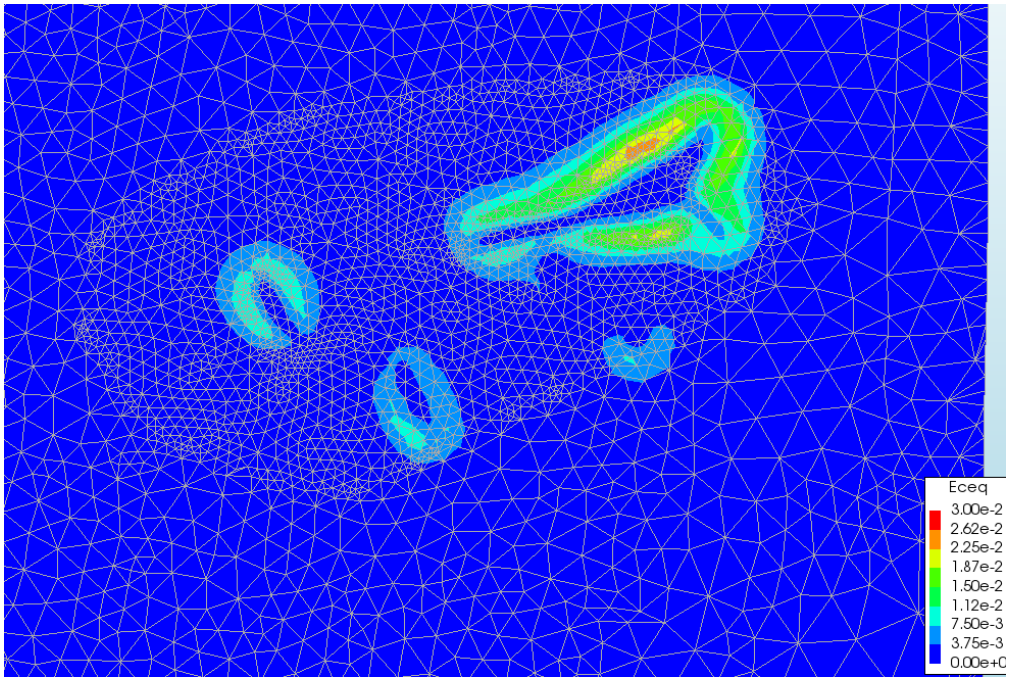

Figure 28: Creep strain in ZE-IV (0-3%) in the post-abandonment phase (2045)

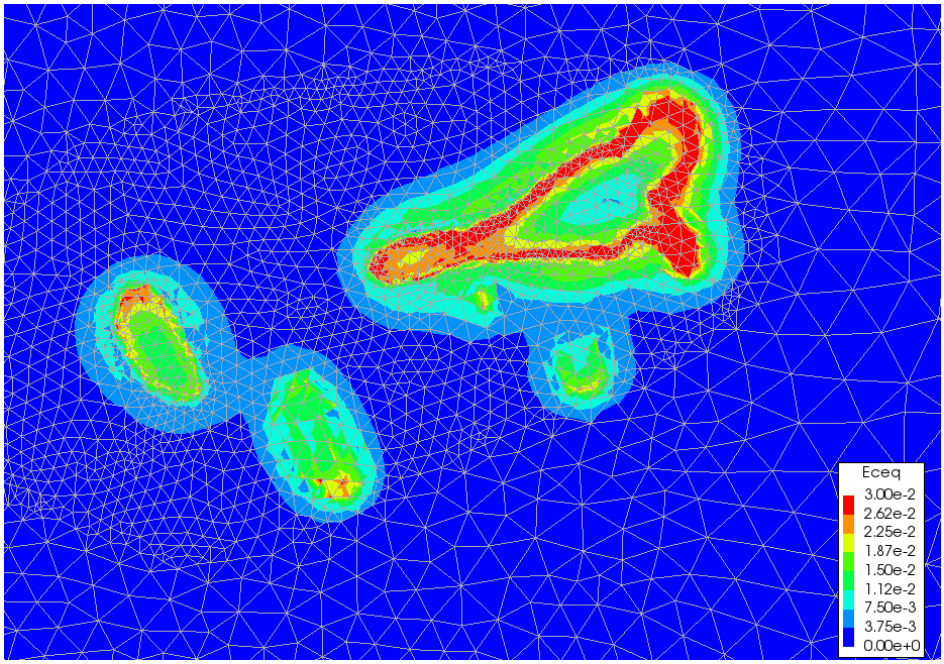

Figure 29: Creep strain in ZE-III-2a (0-3%) in the post-abandonment phase (2045)

3.2 Fracture risks for the ZE-IV halite roof

Similar to the axi-symmetric case, the 3D modelling prior to the April 2018 leakage incident shows a stress reduction in the ZE-IV roof of about 6 MPa; see Figure 30. Given the slightly lower mesh resolution and the use of tetrahedral elements a bit more scattering is seen in the results. Figure 31 shows the pressure and stress evolution, for a (random) element in the ZE-IV salt roof above the cluster. It can be seen that the fluid pressure is higher than the salt stress in 2018, but also after the period of low stress, where the cluster is shut in for abandonment.

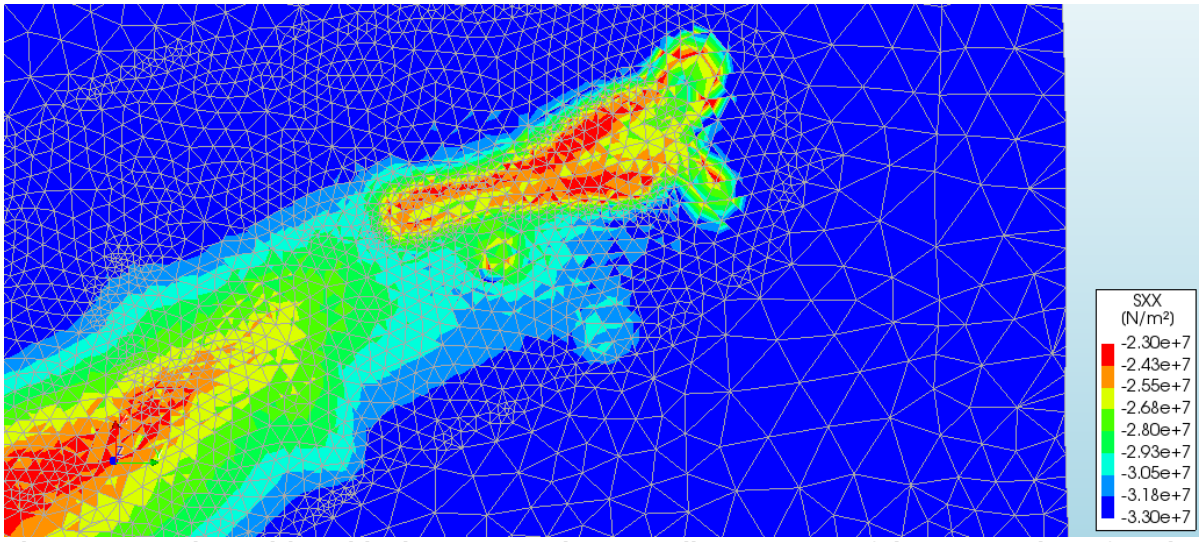

Figure 30: Horizontal (Northing) stresses prior to April 2018 at top of the ZE-IV salt roof. In the middle the red area shows a reduced stress of about 23 MPa, where the vicinity outside the cavern area has level of about 30 MPa, indicating a stress drop of up to 6 MPa since the start of solution mining.

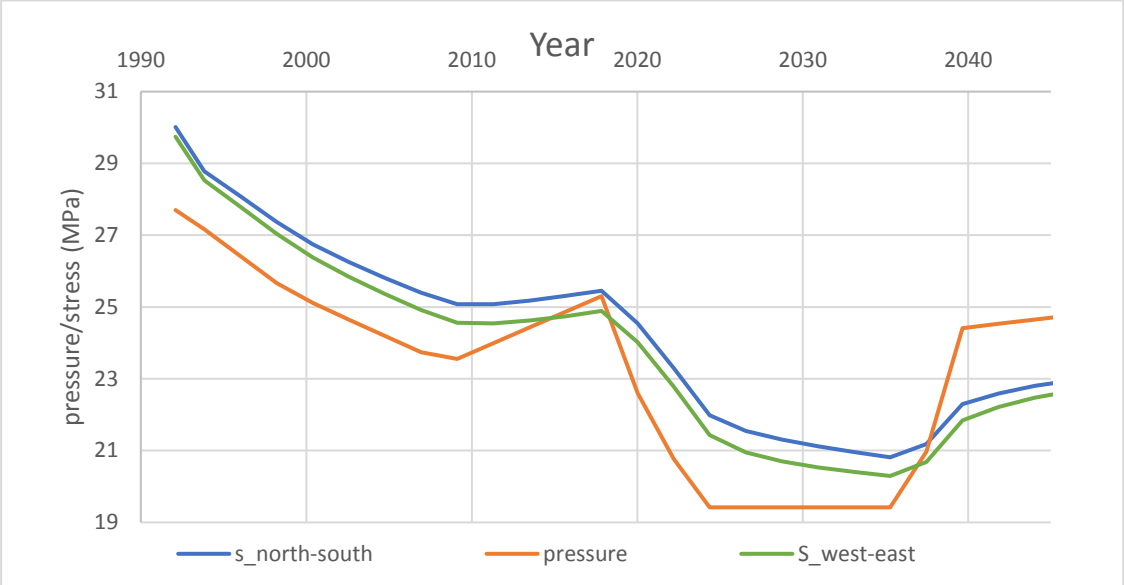

Figure 31: Easting and Northing stress (positive for compression) and pressure evolution for a FEM-element in the top of the ZE-IV salt roof in the middle of the TR-cluster, assuming pressure connection to the cluster. The evolution is slightly different for all the elements (laterally and in depth), so this graph is indicative. For a fracture to develop the fracture threshold needs to be exceeded over the full flow path from cavern to overburden.

After squeezing most of the free brine out of the cluster, and after active mining and convergence in TR-9, VE-3, VE5-6 and VE7-8, a subsidence bowl of about 90 cm is computed (Fig. 32). A realistic time stamp for 90 cm subsidence would be the year 2045, as is adopted by Nedmag in their planning (Fig 35).

When the cluster is closed-in for abandonment at a surface subsidence level of 90 cm and after a prolonged period (11 years) of 12 MPa below lithostatic, the fluid pressures will rise again due to the continuing creep, although the drive for convergence will be much lower, given the lower stress level in the vicinity of the caverns and the effects of precipitates. Pressurisation rates depend largely on the remaining convergence drive at the moment of shut-in for (cavern or cluster) abandonment. Assuming a final production of (on average) 2 m^3/h at 12 MPa sublithostatic stresses, the pressurization towards 9 MPa sublithostatic most likely takes 1-4 years. The pressures in this simulation are enforced, and not the result of convergence of a closed in fluid volume, but the results will be similar in stresses (not time).
The horizontal stresses in the ZE-IV salt roof have decreased by about 9 MPa (Fig. 33), where the simulation assumed a fluid pressure of 6 MPa below lithostatic. It is most likely that this fluid pressure is too high to handle by the cluster, and that fluid is expelled once more via the salt towards the Buntsandstone, levelling off at 8 MPa below lithostatic.

When looking at the stress reductions of the ZE-III-2a (Figure 34), we see a diminished effect of stress reduction with respect to the ZE-IV. This is the effect of the lower stress shielding of the caprock for this layer and/or the dragging effect of the carnallite layer on top of the ZE-III-2a. This effect is irrelevant for caverns that have a developed carnallite section (the TR-cluster and VE-1-2-3) or an open hole connection to the carnallite ZE2b/3b section (TR-9). It will be relevant for the new caverns VE5-6 and VE7-8, although the effect is not a game-changer. The caverns will most likely start leaking after abandonment at 6-7 MPa below lithostatic after a prolonged pressure level of 12 MPa below lithostatic.

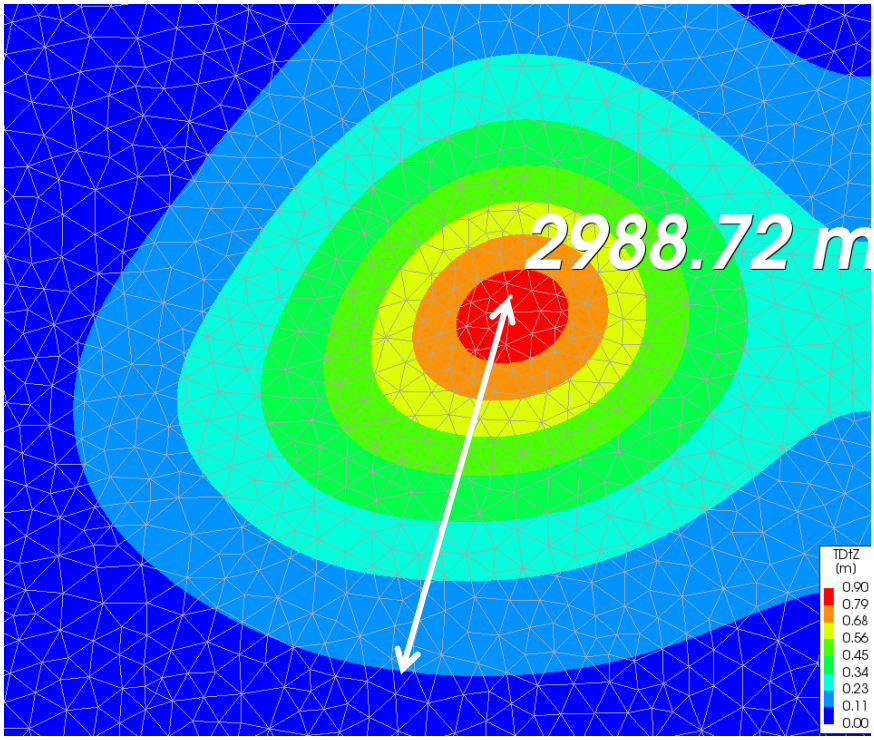

Figure 32: Subsidence 2045 with length bar to indicate the distance between the maximum subsidence and the 10% line, of about 3 km. The effect of VE5-6 and VE7-8 is visible via the small elongation at the west side of the bowl.

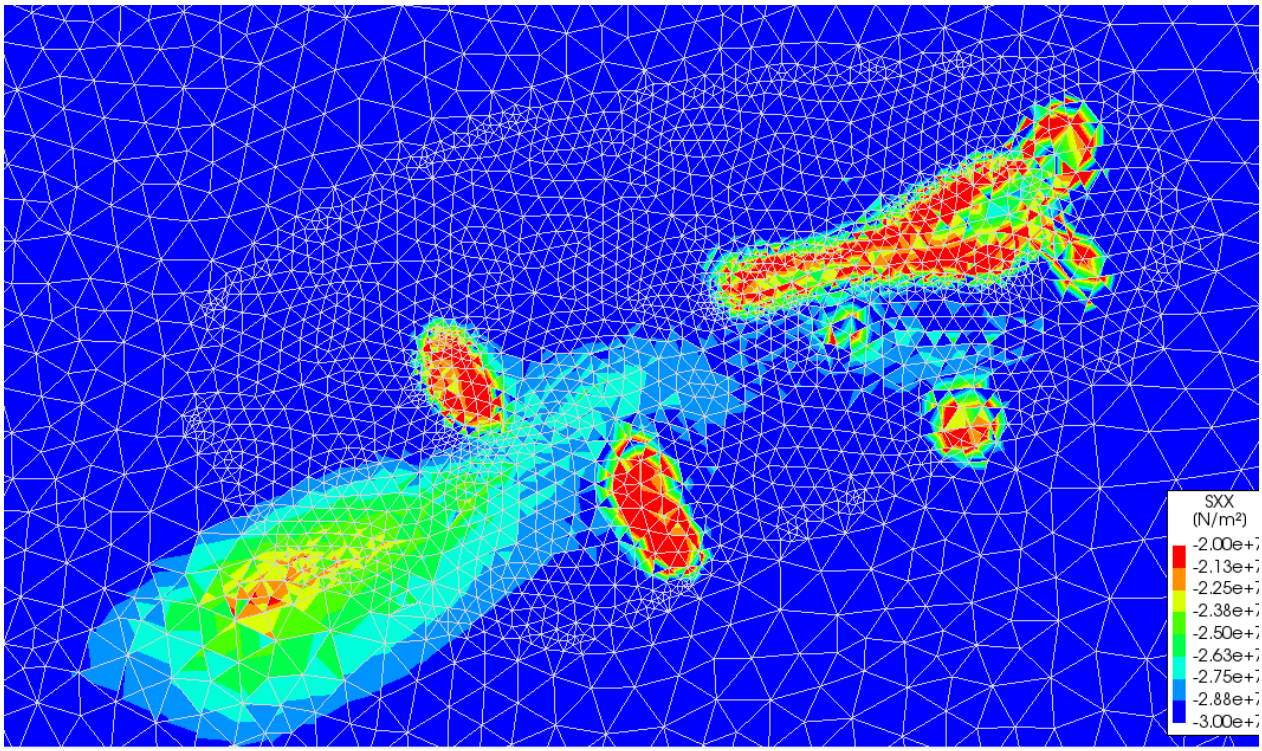

Figure 33: Horizontal (Northing) stresses in the ZE-IV roof after 0.93 m subsidence at a cluster pressure of 6 MPa below lithostatic post abandonment. The salt stresses have decreased by roughly 9 MPa from original lithostatic, indicating that a leakage path most likely is generated. The newly drilled wells have a sublithostatic pressure of 8 MPa (post-abandonment)

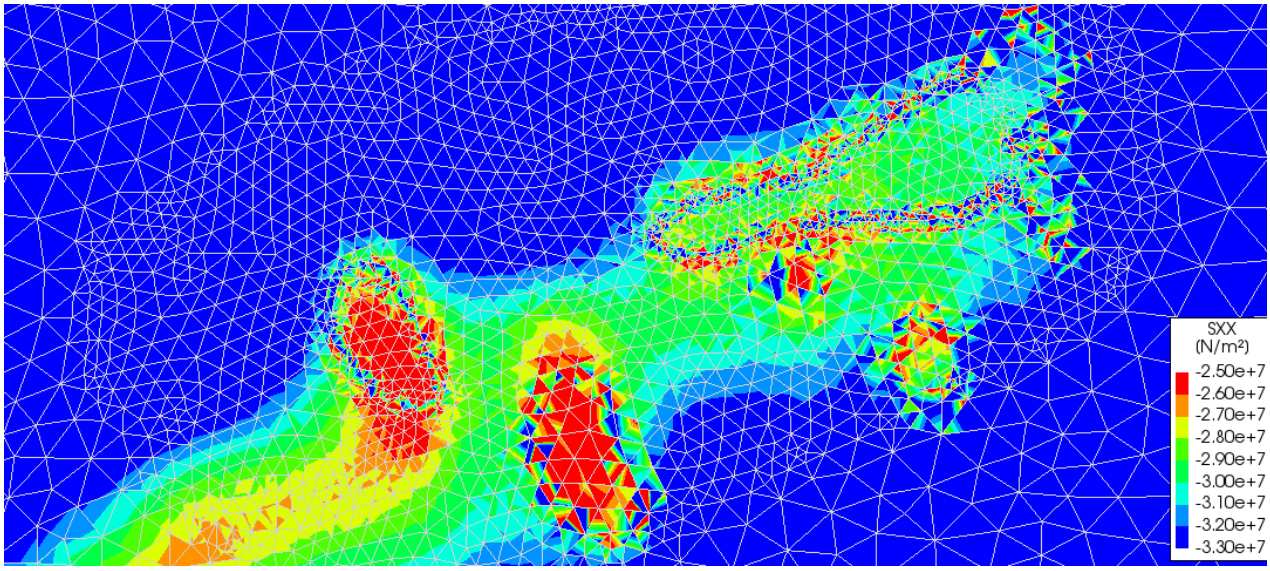

Figure 34: Horizontal (Northing) stresses in the ZE-III-2a roof after 0.9 m subsidence at a cluster pressure of 6 MPa below lithostatic post abandonment. VE-5-6 and VE-7-8 at 8 MPa below lithostatic. The stress reduction is about 6 MPa.

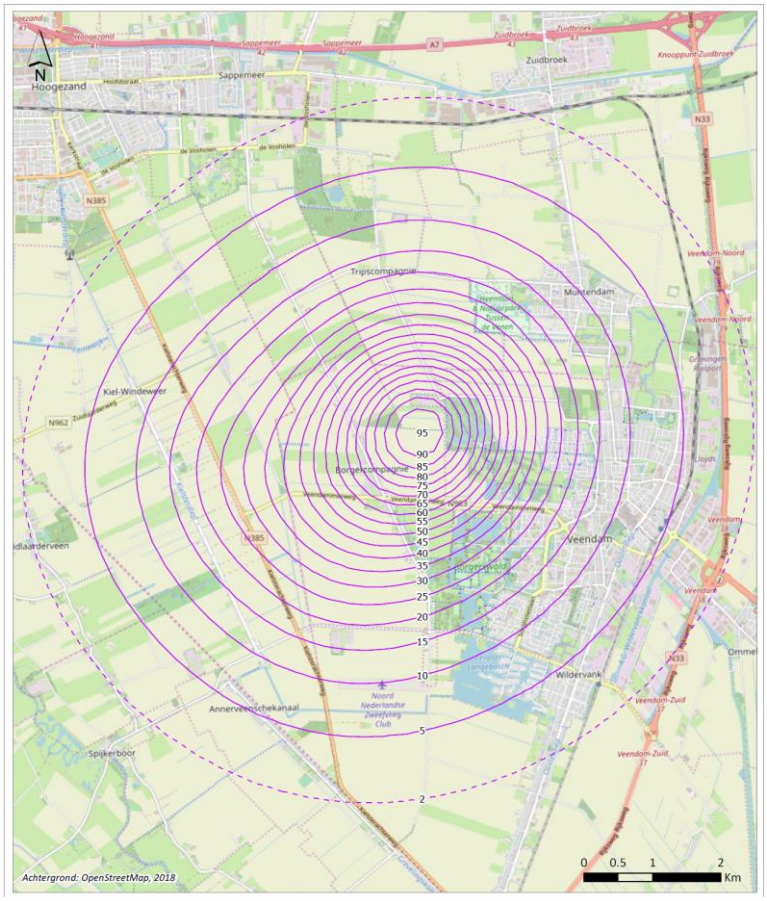

Figure 35 High case subsidence prediction by Nedmag in 2045 with up to 95 cm, displayed in 5 cm intervals

4 General conclusions and recommendations from the 2D and 3D studies

- The minimum and/or horizontal stresses in the halite (ZE-IV) caprock decrease in time due to salt stress relaxation at prolonged sublithostatic fluid pressures. This effect is more or less proportional to the (maximum) level of the sublithostatic pressure and the reduction of the vertical stress level. The influence zone is close to the position of the caverns and radiating out (10% influence) less than 500 m off the cavern edge. The effect is less for caverns that are only developed in the bischofite section (and have a casing shoe in the ZE-III-1a layer), like the planned caverns VE5-6 and VE7-8.

- The cap rock minimum stress (fracture propagation criterion) only returns by a fraction, when the pressure in the cavern is increased again. The small increase is due to an elastic Poisson effect of the pore pressure charging vertically on the cavern roof salt face. In the order of 75% of the long time pressure reduction translates itself in a quasi-permanent reduction of the fracture gradient of the salt roof. This statement is valid for caverns where the lateral extent is (much) larger than the salt roof thickness, which is the case for all full grown caverns of Nedmag.

- The best way to avoid fracture initiation and propagation through the salt caprock (and hence leakage of brine into the caprock) is to allow a declining fluid pressure trend only, until the moment of full abandonment. Abandonment should not occur until the subsurface brine volumes have been reduced to a practical minimum (determined by limited cavern convergence at brine hydrostatic pressure, 11-12 MPa below lithostatic stress).

- The cavern pressure for a cavern in the water injection mining phase should be maximized and having a declining pressure profile in time (cavern volume). The initial pressure should be tuned to the minimum value that follows from vertical density integration (lithostatic level) and the Leak Off Level from the last cemented casing shoe. LOT tests should be mandatory for the last cemented casing. Except for the pre-mining phase as a borehole, where near-lithostatic pressures are required to prevent borehole closure, the active injection pressure level should start at some 90% of lithostatic (from LOT or density integration), equivalent to some 3.5 MPa below lithostatic.

- Adopting an early low fluid pressure regime creates early cavern convergence and too small a cavern to obtain a good quality brine at a sufficient production rate. Assuming that the intent is to connect two caverns (VE-5 with VE-6 and VE-7 with VE-8) a low cavern pressure will also delay the forming of an interconnection.

- As soon as the (mass balance) computed underground brine volume reaches some 450,000 m^3 (or as soon as two caverns connect as intended totaling more than 900,000 m^3 combined), the pressure should be slowly lowered to 8-9 MPa sublithostatic at a pace which is determined (by mass balance) to reach a balance of growth by dissolution and creep convergence. The pressure drop can be tuned somewhat with the (measured) effects on convergence rate, cavern interconnectivity and brine quality. The total (free) brine volume of intended interconnections should preferably be kept at a volume that is more manageable in case of incidents. A maximum for the total free (squeezable) brine volume of 1.5 million m^3 per intended set (VE5-6 and VE-7-8) or single cavern (VE-3 and TR-9) seems a reasonable limit to adopt. If this limit is approached the production should be increased or the injection decreased, automatically lowering the cavern pressure and volume in time.

The lower brine volumes and lower pressures will not allow an incident to occur that approaches the same order as the incident with the cluster in April 2018.

- Due to non-constant brine demands (Nedmag use and sales, potential tubing defects (that require time to repair) and fluctuating rainwater volumes, some pressure fluctuations can and should be allowed. A practical way would be to determine the minimum year-average pressure history of a cavern and set a maximum pressure level of 1.5 MPa (per cavern or connected set) above that level. In case this level is reached, a mandatory pressure bleed-off should be performed. In emergencies the brine should be externally stored in tanks or basins, or (less preferable) disposed of towards the sea. The same holds true for an excess of rain water. These options have been created in 2018 as a learning point from the leakage incident.

- For large caverns (>500.000 m^3 free brine volume) it is most likely practical to have (a minimum of) two wells into it. It allows injection and production from different wells, increasing the brine quality and decreasing levels of corrosion and crystallization (the latter by simultaneous (cold) water injection and (hot) brine production). It also decreases the risk that production is hampered for many months due to a broken off tubing set, awaiting a work-over to be performed (availability issue)

5 The effect of post abandonment leak-off of caverns by fracturing (with a pressure drop)

When fluid pressures exceed the rock stresses, a fracture can be created. Branched fractures or a permeation system on microscale will give a gradual leak-off that will balance salt inflow, but a single fracture can give pressure pulses, that have the potential to also fracture low permeable rocks on top of the salts, driving brine (and potentially diesel floating on top of the brine) into the shallower overburden layers. For pollution of sweet water aquifers a fracture must grow to the top 250 meters of soil (for brine) or (for oil that can move up by buoyancy in water) past the clay layers on top of the Chalk. How high a fracture can grow is a function of the volumes that can be stored in the fracture itself and the volumes that can leak off into the permeable formations.

At the leakage incident that started 20 April 2018, a fracture created a pathway between the cavern cluster and the overburden. The pressure dropped 10 bars over 30 minutes and 30 bars during 48 hours, after which the pressure stabilized. Most likely 75000 m^3 leaked off in the first two days due to elastic effects mainly and 25000 m^3 in the days hereafter by creep effects mainly, totaling 100,000 m^3 before the fracture was apparently closed again. The amount of leakage can only be estimated if the stiffness of the system is known, where the creep only contributes to small amounts over a few days. During the years prior to the incident, 2-4 bar pressure cycles also occurred due to varying demands of brine or increased rainwater injection at periods of heavy rainfall. Based on these, cycles, the TR-cluster compressibility was computed to be between 1700 and 3200 m^3/bar (P10-P90 case) with a P60 of 2500 m^3/bar. The uncertainty is mainly caused by the inaccuracy of historic data recording of pressures (rounded to 1 bar) and the longer intervals of recording (monthly basis) at which creep volumes are not negligible anymore with respect to elastic expansion volumes for 2-4 bar.

For the incident, Panterra (P. v.d. Hoek Oct 2018) have performed fracture studies to estimate in which formations the fracture may have ended up. The most critical are the first hours to first days, where high fluid flows exist, of which only a fraction can flow into the low and medium permeability formations at depths exceeding 400 m. The largest uncertainties in the study are the very limited set of permeability data. Most data have been derived from scarce Nlog data. The best estimate of the study was that the fracture did not reach the sweet water layers (0-250 m), which is supported by the absence of magnesium or oil pollution of water quality measurements from shallow (10-20 m) to deep (120 m) water producing (or sampling) wells during the half a year after the incident.

The intention is to reduce the brine volume in the caverns as much a practically possible by keeping the cavern pressure close to brine-hydrostatic for some 10 years or so, until the squeeze brine flow is less than an assumed 2 m^3/h on average. It is assumed that most of the free bischofite brine has been squeezed out and about half of the free carnallitic cavern brine (for caverns that have a developed ZE-III2b/3b section: TR-1 until TR-7 and VE-1 until VE-4). How much brine can be squeezed out exactly (and high much brine is left behind at abandonment) highly depends on the support behavior of precipitates, hindering the inflow of bischofite and other salts. It is assumed that 100.000 m^3 of “free” bischofite brine is left per cavern cluster, together with the bound brine in the precipitates and half of the carnallitic brine. The largest remaining brine volumes (by far) are estimated to be in the present cavern cluster (TR-1 to TR-8 and VE-4).

These assumptions on remaining volumes can and will be quantified in much greater detail at the moment of cavern abandonment (prior to the abandonment of the last well leading to a cavern cluster). Also the cavern stiffness can be measured at this stage by performing a pressure cycle test. It is not likely that larger caverns will be abandoned in the coming 5-10 years, so that this exercise merely serves as an early estimate for post-abandonment behaviour and not as a

detailed abandonment plan, which will be submitted to the Inspectorate on Mines prior to submitting a proposal to close off the last remaining well.

After caverns have been abandoned by setting a cement plug in the last remaining access well, the pressure in the cavern will build up slowly because of the remaining squeeze potential (even when as low as 0.1-1 m^3/h). At some moment in time the pressure will exceed the stresses in the salt caprock. Although gradual leakage can occur by micro-permeation, the worst case situation is a sudden fracture that bleeds off a volume of brine from elastic expansion of brine and elastic contraction of the cavern walls. This worst case situation has been analyzed by PanTerra (P. van den Hoek), Analysis of post abandonment leakage from caverns of cavern clusters, November 2018,

Taking an analogy from the cluster incident it is assumed that the brine pressure drops by 3 MPa, of which 1 MPa in 30 minutes and another 2 MPa over 48 hours. The elastic volume has been scaled with the remaining brine volume. Since most (90%) of the elastic volumes are caused by cavern wall contraction, it is assumed that the precipitates will support the cavern walls to some extent for the bound brine in the precipitates, where they will not for the remaining free brine. A reduction factor of 50% was chosen for the bound brine. This division was also taken for the cavern cluster in 2018, so that a compressibility for free and bound volume could be determined. This distribution can be verified only at the time that a (once) larger cavern is close to abandonment.

The estimated post-abandonment volumes are summarized in table 1 and they have been given an elastic brine expulsion volume, based on the brine expansion and cavern contraction for a pressure drop of (a total amount of) 1 and 3 MPa respectively.

	free 2b/3b brine at time of abandonment	bound brine at time of abandoment	compressibility	outflow 1st half hour	ouflow 0.5 - 48 hours
	M(m^3)	M(m^3)	m^3/bar per M(m^3)	m^3	m^3
Cluster	0,495	3,76	1104	11039	22077
TR-9	0	0,27	105	1048	2096
VE-1 (no 1b cavern)	0,025	0,12	38	379	758
VE-2	0,02	0,16	89	892	1784
VE-3	0,035	0,63	201	2007	4014
VE-2 + -3	0,055	0,79	245	2453	4906
VE-5 + -6	0	0,48	152	1516	3033
VE-7 + -8	0	0,37	127	1271	2542

Table 1: Estimated brine volumes in the caverns at abandonment.

The volumes have been taken as input for a fracture propagation study for the cavern (clusters) as in Table 2:

- TR-cluster (TR-1 to 8 and VE-4)
- VE5-6 (also representing the somewhat smaller VE7-8 and TR-9)
- VE2-3 (assuming a future interconnection)

	outflow 1st half hour	ouflow 0.5- 48 h	Init. frac depth	viscosity brine	density brine
	m^3	m^3		mPa.s	kg/l
cluster	11000	22000	top 3b	3.1	1.3
VE-5/-6 (also repr VE-7/-8 and TR-9)	1500	3000	top 1b	5.7	1.35
VE-2/3	2500	5000	top 3b	3.1	1.3

Table 2: Estimated outflow volumes post-abandonment at the first 30 minutes (1 MPa pressure drop) and subsequent 47.5 hours (additional 2 MPa pressure drop).

The cavern VE-1 (with only a ZE-III2b-3b section) is considered to be so small that its fracture propagation potential is much smaller than for the rest.

The best estimate minimum stress profile has been taken from the previous study (v.d Hoek; Okt 2018), regarding the leakage incident and is plotted in Figure 36.

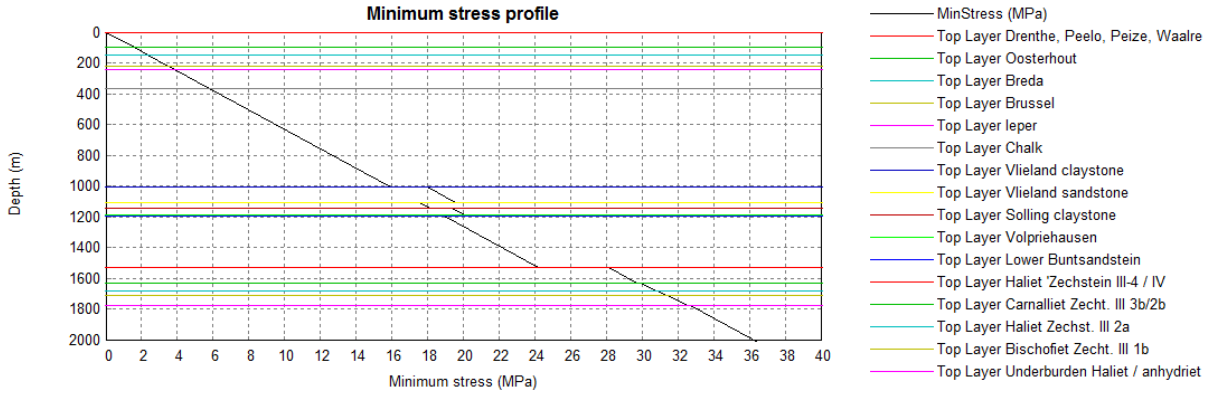

Figure 36: best guess minimum stress as a function of depth and lithology

The permeability of most overburden rocks is low (0.1-10 mD), with outliers in the Vlieland sand and shallow sands, see Figure 37. Especially for the 48 hours timeframe, even low (1mD) permeability rocks are able to take in brine, but for the first 30 minutes, only permeable sands will take up significant volumes where the bulk of the brine is (temporarily) stored within the fracture itself. Please note that, based on research, permeabilities for the Breda and Vlieland sandstone layer have been adjusted from the study by PanTerra (Paul van den Hoek) from October 2018.

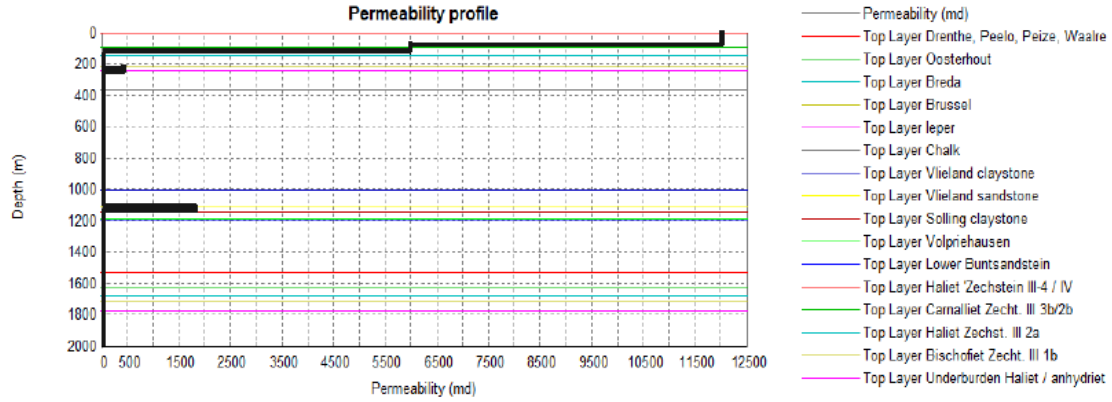

Figure 37: Permeability (in mD) as a function of depth and lithology

The fracture growth for the post-abandonment cluster is shown in Figure 38, where it is expected that a fracture grows towards the Vlieland sands in about 20 minutes and stops growing beneath the Vlieland Claystone. The subsequent leakage over 48 hours with a highly reduced flow rate does not change the fracture dimensions

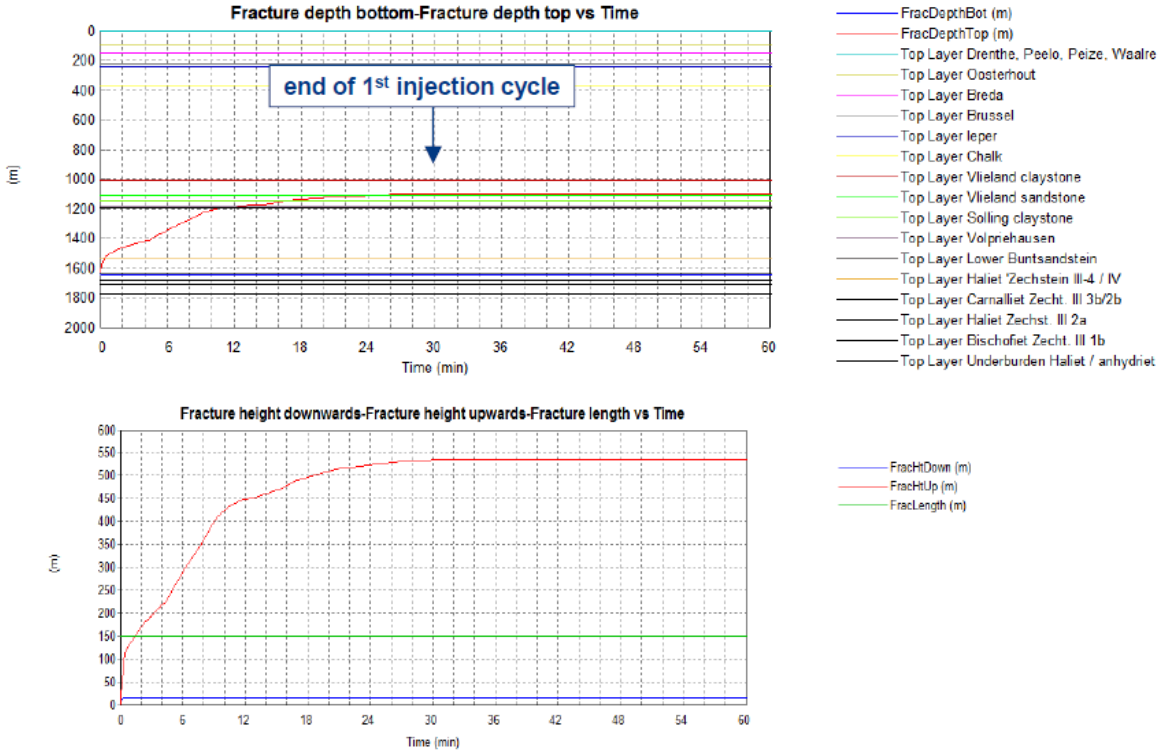

Figure 38: Fracture growth (in height) for the TR-cluster

A similar computation was performed for cavern cluster VE5-6, where the total volume of brine is much smaller than for the TR-cluster, see Figure 39. In this case the volumes are not sufficient to create a fracture towards the Vlieland sand. Since VE5-6 only contains bischofitic brine (with a density of 1.35 kg/l versus 1.30 kg/l for carnallitic brine), the increased density will also have helped to keep the fracture growth in upward direction limited.

For the (potential) cluster VE2-3, the simulations also predict that the fracture will not propagate beyond the Buntsandstone, see Fig 40.

The simulations show that the post-abandonment caverns may create fractures into the Vlieland sand for the (still large volume) TR-cluster, but not for the smaller caverns VE5-6. The even (expected) smaller caverns VE7-8 and TR-9 will also not reach the Vlieland sands.

The worst case leakage for abandoned caverns is hence much smaller than the leakage incident of April 2018. It is however advised to re-iterate these computations (just) prior to moment of abandonment, with improved information on elastic cavern stiffness components and creep convergence rates, potentially also incorporating new found data on permeability and in-situ stress data or incorporating new learnings from the April 2018 leakage incident.

More detailed information on the fracture computations can be found in V.d.Hoek (nov 2018).

The risk of fault reactivation by temporary pressure increases in the overburden also seems much smaller, compared to the April 2018 incident because of the smaller volumes of brine and lower potential pressurisation. The fault reactivation risk is addressed by Urai (Nov 2018).

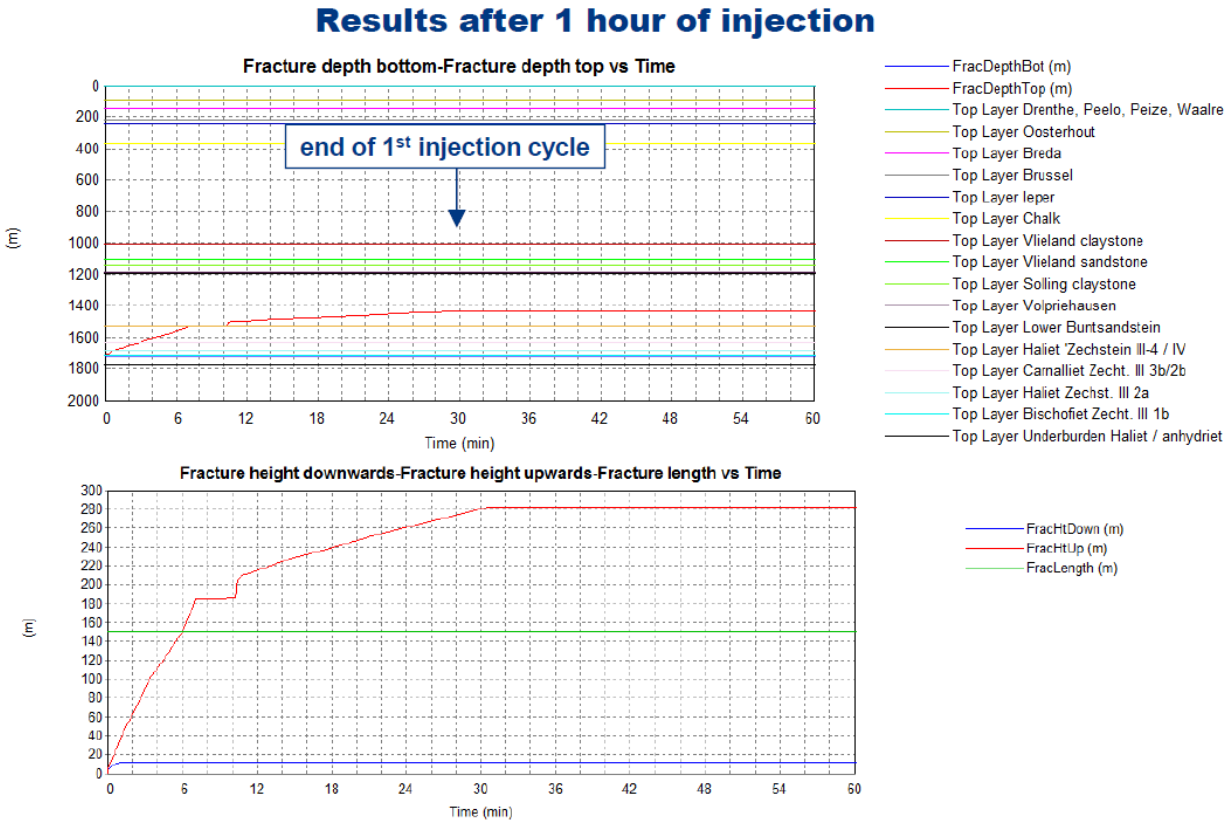

Figure 39: Fracture growth (in height) for VE-5/6, where the fracture tip is not expected to reach the Vlieland sands.

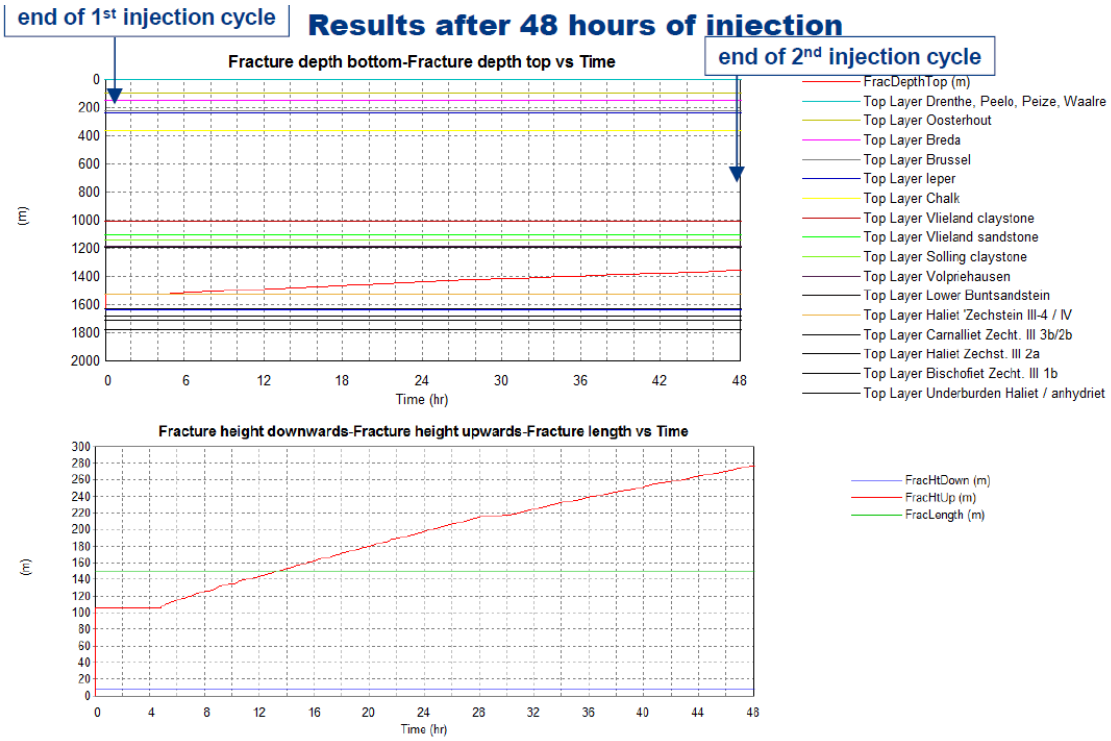

Figure 40: Fracture growth (in height) for VE2-3, where the fracture tip is not expected to reach the Vlieland sands.

6 Conclusions for cavern integrity due to fracturing

The general learning of this study is that salt stresses decrease in time for caverns with a large diameter with respect to the thickness of the (salt) caprock. Caverns that are operated under low fluid pressures build up arching stresses around the cavern that can be creep relaxed in time, transferring the arching stresses to the elastic layers above the salt, in this case the Buntsandstone. This process in not (or hardly) reversible, so that the caprock can be fractured at brine pressures (far) below the original lithostatic brine pressures.

Simulations have been performed that are in line with all the measurements (convergence rates, subsidence, leakage point) and can serve to predict the behaviour of the cavern cluster (that will go into a mode of low pressure cavern convergence), the remaining existing caverns and the caverns that are planned to be drilled in the coming years (VE5-6 and VE7-8)

By adopting a strategy of slowly reducing brine pressures in the caverns, the situation of fluid pressures exceeding the minimum salt stresses (a prerequisite for fracturing) can be avoided during the period of active salt mining. New caverns can be developed at (relatively) high fluid pressure in order to allow fast brine volume growth (and fast brine saturation towards brine qualities that can be used commercially), and a gradual reduction in pressure to limit the cavern growth and (final) volume at a later stage.

The last stage is a period of low pressure brine production (and no water injection), in which the volume of the cavern is reduced to a practical minimum, where most of remaining brine will be locked in by precipitates.

At some moment in time (for a suggested 2 m^3/h brine production minimum) caverns need to be abandoned by placing a cement plug in the (last access) well of the cavern. The low remaining convergence rate will pressurize the cavern in time, where brine pressures will exceed the minimum salt stresses. It is possible that leakage will happen by micro-permeation and that convergence and leakage are in balance (at 0.1-0.5 m^3/h for a pressure level well above the brine-hydrostatic pressure), but it also possible that leakage will occur intermittent by opening and closing fractures. In this case, larger volumes of brine leak into the overburden in a short time, which can create fractures that allow brine to flow to shallower formations, despite the high brine density compared to formation brines. The brine can be contaminated with diesel oil, which was either trapped in the top section of the cavern (near the fracture start) or diesel oil that has somehow escaped from the deeper pockets of the caverns and was able to find its way to the upper section of the cavern.

A study by Panterra (v.d. Hoek, Nov 2018), showed that for the present and future caverns it is unlikely that post abandonment fractures pass the Vlieland Claystone, given the brine volumes involved. Pollution of shallow layers with magnesium brine and potentially diesel is therefore very unlikely. Especially when it is kept in mind that during the 7 months after the leakage incident of April 2018, no traces of (magnesium-enriched) brine or oil were found in all of the monitoring wells in the vicinity of the brine field.

References

Raith, A., Urai, J.L. (Dec 2016): Squeeze mining-induced stress changes in the faulted overburden of the Veendam salt pillow.
Urai, J.L. (Nov 2018): Nedmag Winningsplan 2018 Squeeze mining-induced stress changes in the faulted overburden of the Veendam salt Pillow.
Urai, J.L. (1983): Deformation of wet salt rock; thesis; university of Utrecht (Netherlands).
Urai, J.L. (1983): Water assisted dynamic recrystallization and weakening in polycrystalline bischofite. Tectonophysics 96, 125–157.
Fokker, P.A. (1995): The behaviour of salt and salt caverns. Dissertation, Delft University of Technology; Netherlands.
Hoek, P. v.d. (Oct 2018): Analysis of VE/TR salt cavern cluster leakage incident of 20 April 2018. PanTerra Geoconsultants B.V.
Hoek, P. v.d. (Nov 2018): Analysis of post abandonment leakage from caverns or cavern clusters PanTerra Geoconsultants B.V.
Fokker, P.A. (July 2018): Evaluatie oorzaak pekellekkage in Nedmag pekelcluster 20 april 2018 – update juli.

Appendix 1 Material Parameters Finite Element study

Material parameters applied in the 2D (axi-symmetric) and 3D simulations. Stiffness parameters are in Pa. Density is in kg/m^3. Creep parameters A (first entry) are in s^{-1} for a reference Von Mises stress of 1 MPa. The K0 is the target initial stress level as ratio of total horizontal stress over total vertical stress.

Axi-symmetric:

	density g/cc	Young M GPa	Poisson	n	A /s	K0 Sh/Sv
North-Sea (topsoil)	2.1	0.5	0.4			0.8
Cretateous	2.3	5	0.3			0.8
Triassic/Bunter	2.3	12	0.3			0.75
Halite ZE-II	2.2	20	0.3	4	1.E-13	1
Halite ZE-III-IV	2.2	20	0.3	4	1.E-14	1
Mg-salts	1.7	3	0.3	2	5.E-13	1
ZE-I / Rotliegend	2.3	10	0.3			1

3D-modelling:

	density g/cc	Young M GPa	Poisson	n	A /s	K0 Sh/Sv
Quaternary/	2.1	0.5	0.4			0.7
Cretaceous	2.3	5	0.3			0.7
Rot	2.25	9	0.3			0.7
Triassic/Bunter	2.3	12	0.3			0.75
Halite ZE-II	2.2	20	0.3	4	1.E-13	1
Halite ZE-III-IV	2.2	20	0.3	4	1.E-14	1
Carnallite	1.7	3	0.3	2	5.E-13	1
Bischofite	1.7	3	0.3	1.6	6.E-13	1
ZE-I / Rotliegend	2.3	20	0.3			1